Advances in Water Resources 162 (2022) 104140

Contents lists available at ScienceDirect

Advances in Water Resources

journal homepage: www.elsevier.com/locate/advwatres

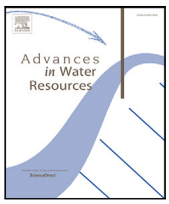

Dimensional reduction of a fractured medium for a two-phase flow

Martin Dugstad *, Kundan Kumar

Department of Mathematics, University of Bergen, Bergen, Norway

ARTICLE INFO

Keywords:
Fractured porous media
Upscaling
Two-phase flow

ABSTRACT

We consider a porous medium containing a single fracture, and identify the aperture to length ratio as the small parameter ϵ with the fracture permeability and the fracture porosity scaled as exponents of ϵ. We consider a two-phase flow where the flow is governed by the mass balance and the Darcy law. Using formal asymptotic approach, we derive a catalogue of reduced models as the vanishing limit of ϵ. Our derivation provides new models in a hybrid-dimensional setting as well as models which exhibit two-scale behaviour. Several numerical examples confirm the theoretical derivations and provide additional insight.

1. Introduction

Fractures are in abundance in the subsurface such as soils (National Research Council et al., 2001; Smith et al., 2003; Watanabe et al., 1998), in glaciers (Fountain and Walder, 1998), and in many other types of porous media such as wood and concrete (Carmeliet et al., 2004). Fractures are discontinuities in the medium that form narrow zones where the hydraulic properties such as permeability or porosity are strongly different from the surrounding matrix. The fractures have a strong influence on flow and transport, either making flow in certain directions several orders of magnitude more rapid than in other directions or possibly nearly blocking flow in certain directions. In cases where the fracture is highly permeable it can act as the dominant flow pathway through a porous matrix where there is almost no flow in the porous matrix, or in cases with low permeability in the fracture it may act as an barrier allowing no fluids to pass through (Adler and Thovert, 1999). Taking them into account therefore is of great interest in a wide variety of applications. For instance, in the petroleum extraction, a fracture can lead to enhanced oil production, or in CO_2 storage applications it can act as a leakage pathway. Therefore, the effects of fractures or entire fracture network need to be incorporated in mathematical models for fluid flow and transport.

There is a rich literature dealing with fractures and we refer to textbooks (Bear, 1988; Helmig et al., 1997; Adler et al., 2012) as standard references and to Berre et al. (2019) for a recent survey. The fracture has a small aperture to length ratio, and this makes it difficult to resolve the fluid flow explicitly through brute force computations. This is evident as the thinner the fracture is, one requires smaller grid size to resolve it. In most cases, this is also not of much use as the transverse flow details may not be important in a thin medium. Given that the resolution of the fracture by discretizing the thin and long medium is computationally infeasible, we are left with alternative approaches to account for their impact. Several approaches exist that account for this impact and we refer to a recent survey (Berre et al., 2019) where they describe some of the most known methods.

There are two wider classes in which we can classify the methods to take the fractures into account. One is the continuum type models where the effects of fractures are incorporated by suitably modifying the matrix hydraulic properties (Gerritsen and Durlofsky, 2005; Arbogast et al., 1990), and the second discrete fracture network or mixed dimensional models where the fractures are embedded as a lower dimensional objects in a porous matrix. The second class of methods relies on explicit representation of fractures but representing them as lower dimensional geometric objects embedded in a three dimensional porous matrix. Due to the huge number and a large variation in the shapes and sizes of the fractures in a real porous medium, it is not possible to resolve all the fractures. A compromise is achieved by explicitly representing only the most dominant fractures and incorporating the smaller ones in terms of effective hydraulic properties as in the continuum models. The variant of these approaches are known as discrete fracture matrix model (DFM), Discrete fracture network models (DFN), reduced models, or more generally as mixed-dimensional models. This has been widely used (Bastian et al., 2000; Reichenberger et al., 2006; Fumagalli and Scotti, 2013; Aghili et al., 2019) for a variety of flow models, and Singh et al. (2014), Girault et al. (2016), Bukac et al. (2016), Bukač et al. (2015), Andersen and Evje (2016), Brenner et al. (2018) for multiphysics models including geomechanics and other advanced physical models. The advantage of this method is a more faithful representation of the fracture network geometry but the challenges are in dealing with the amount of geometric complexity contained within discretized grid block and the effect of strong heterogeneity

* Corresponding author.
E-mail address: mdu055@uib.no (M. Dugstad).

https://doi.org/10.1016/j.advwatres.2022.104140
Received 12 August 2021; Received in revised form 20 January 2022; Accepted 24 January 2022
Available online 25 February 2022

of the fracture-matrix properties, for instance discontinuities in matrix pressure across the fracture caused by resistance to flow. The setting of this paper is in the second class of method.

The particularity of our setting is an immiscible two-phase flow model widely used in the multiphase flow problems where two or more fluids share the pore-scape. The interplay of capillary, viscous, and buoyancy forces for the fluids in a complex pore geometry leads to a nonlinear, possibly degenerate system of partial differential equations modelling the flow behaviour. Standard textbooks e.g., Bear (1988) discuss these flow equations and are standard in porous media flow studies. Our work deals with the effective models that explicitly represents the fractures and focusses on the effect of heterogeneities in the fracture-matrix properties. In particular, we use formal asymptotic approach to provide a rational derivation of the variety of effective models that result for different regimes of this heterogeneity. The starting model is an equi-dimensional one for the fracture and the matrix where the fracture is represented as a thin domain with a non-zero thickness with the standard two-phase Darcy equations describing the flow in both the fracture and matrix. The use of standard two-phase Darcy model for the fracture is premised on the fact that the fracture is also assumed to be porous though possibly with drastically different hydraulic properties. Natural interface conditions of the continuity of pressure and fluxes are imposed at the matrix–fracture interfaces. One of the new difficulties that comes with a two-phase flow model is the different relative permeability and the capillary pressure curves for flow in the fracture and in the matrix. Roughly speaking, our work here derives effective models as the limit of the thickness of fracture vanishes leading to reduced order models where the fracture becomes effectively a lower dimensional geometric object. We focus on the derivation of these effective models.

This work connects the surrounding matrix which is solved by a flow equation with a fracture that is solved using a differential equation on the lower dimensional fracture surface. These fracture can, depending on their properties, act as barriers, open fracture or something in between. This suggests that the upscaled models should distinguish between these cases. The key parameter in our approach is ε, the ratio of the width to the length of the fracture. The porosity and the permeability contrast of the fracture-matrix heterogeneity is then taken as the scale of ε as follows:

$$\frac{\phi_f}{\phi_m} \propto \varepsilon^{\kappa} \quad \text{and} \quad \frac{\hat{K}_{a,f}}{\hat{K}_{a,m}} \propto \varepsilon^{\lambda}.$$

Here, $\phi_f, \hat{K}_{a,f}$ and $\phi_m, \hat{K}_{a,m}$ are the porosities, absolute permeabilities of the fracture and the matrix, respectively. Our assumption for the starting model is of Darcy type in both the fracture and the matrix. This corresponds to the situation when the fracture is filled with some material so that we assume the model equations are of the same type in both the subdomains. The two parameters κ and λ determine the contrast of hydraulic properties of matrix versus those of the fracture. Our approach is to derive effective models as ε goes towards zero for different values of the parameters κ and λ. In contrast to the single phase flow, here the relative permeability and the capillary pressure curves may be different in the fracture and the matrix. Though we consider a single fracture, following Formaggia et al. (2014) our work can be used to provide a hierarchy of reduced models based on the properties of the fractured networks.

Our approach uses formal asymptotics for the derivation of upscaled models. These upscaled models are the equations satisfied by the leading order term in the expansion of the solution variables. Similar works pertaining to the derivation of upscaling of models for fractured medium have been followed in Dugstad et al. (2021) and Kumar et al. (2020). In Dugstad et al. (2021) they explore the effects of polymer in a fracture case where the permeability of the fracture is scaled with the width of the fracture. Moreover, the permeability is supposed to be anisotropic and the effective models are obtained as a result of the scalings for the diagonal permeability components. A closer reference to the present work is Kumar et al. (2020) where similar effective models but for the Richards equation have been obtained. The similarity is closer here as in the present case both the porosity and the permeability are scaled as the exponents of ε. Here, we follow a similar approach but for an immiscible two-phase flow containing oil and water. The two-phase flow model is the standard multiphase flow widely used in the subsurface energy and environmental applications and in the fractured context, it has also been widely used in the literature, see e.g., (Bastian et al., 2000; Pruess and Narasimhan, 1982) where they study two-phase flow in a fractured porous medium. Surprisingly though, there are far fewer results on the derivation of effective models. The closest to our situation is Ahmed et al. (2017) where reduced models are derived for two-phase flow models. However, the approach there is quite distinct from the ones we follow. Their approach is inspired from the analogous work in the single phase flow case as performed in Martin et al. (2005). Our results are consistent with their results in certain regimes of the permeability. We make this comparison later in the Remark 3.1. In contrast to a formal approach here, a rigorous mathematical approach has been widely used in literature. We refer to the works of Morales and Showalter (2010, 2012), Tunc (2012) for a single phase flow. In case of the Richards equation we refer to List et al. (2020) where mathematically rigorous convergence results are obtained for a certain range of parameters. For a study on the transport equation in similar setting we refer to the work by Pop et al. (2017). Gander et al. (2021) uses Fourier analysis to obtain coupling conditions between subdomains and obtain model error estimates when the fracture is represented as a hypersurface embedded in the surrounded rock matrix. In Neuss-Radu and Jäger (2007), Gahn et al. (2018, 2016), the authors consider a thin domain with periodic coefficients for a reactive transport model and perform a rigorous two-scale homogenization to obtain interface conditions.

The numerical methods for solving multiphase flow in a fractured medium has received more attention. We refer to the literature (Hoteit and Firoozabadi, 2008; Fumagalli and Scotti, 2013; Kim and Deo, 2000; Fumagalli et al., 2019; Brenner et al., 2015; Angot et al., 2009) and the recent review of Berre et al. (2019) for a discussion on the numerical methods for solving the reduced models for two-phase flow. A typical approach is using domain decomposition and mortar variables for the fracture variables. In the present work, we will use three different models which treat the fracture in different ways. One model where the fracture is treated as a lower dimensional object, one "two scaled model" where the fracture is rescaled into a separate domain and one model where the fracture acts as an barrier where there is zero flux over the fracture

The paper is structured as follows. In Section 2, we introduce our two-phase flow model where we work with a non-degenerate case. In Section 3 we give a catalogue of the effective models for different permeability and porosity in the fracture. In Section 4 we derive our effective models. Here, we use a formal asymptotic approach and obtain upscaled models for the different regimes of parameters κ and λ. In Section 5 we introduce our numerical results which illustrate the quality of our upscaled models and in the last section we state our conclusions regarding the upscaled models and the numerical simulations.

2. Model equations and scaling

First we formulate the models in a dimensional form. Let $\hat{\Omega} \subset \mathbb{R}^2$ be an open, bounded, and convex polygonal domain with boundaries denoted by $\partial\hat{\Omega}$. The domain contains a single fracture $\hat{\Omega}_f$ which divides $\hat{\Omega}$ into two subdomains $\hat{\Omega}_1$ and $\hat{\Omega}_2$. We get that $\hat{\Omega} = \hat{\Omega}_1 \cup \hat{\Omega}_2 \cup \hat{\Omega}_f$, and that $\hat{\Omega} \backslash \bar{\Omega}_f = \hat{\Omega}_1 \cup \hat{\Omega}_2$. The interfaces between the subdomains are denoted by $\hat{\Gamma}_1 = \partial\hat{\Omega}_1 \cap \partial\hat{\Omega}_f$ and $\hat{\Gamma}_2 = \partial\hat{\Omega}_2 \cap \partial\hat{\Omega}_f$. We reduce the fracture domain to be a one-dimensional interface between the two domains $\hat{\Omega}_1$ and $\hat{\Omega}_2$.

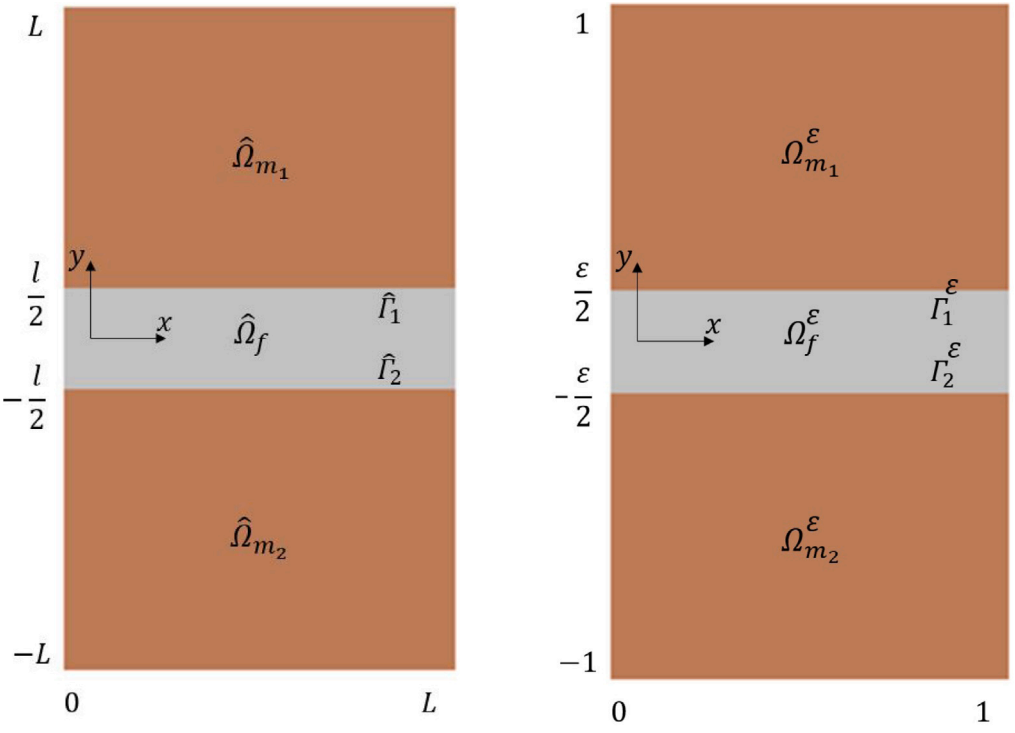

(a) The domain $\hat{\Omega}$ in dimensional form. (b) The domain Ω in non-dimensional form.

Fig. 1. Dimensional domain $\hat{\Omega}$ and dimensionless domain Ω. Both domains have a fracture between two matrix blocks.

2.1. Dimensional model

We simplify the geometry so that the fracture boundaries are straight lines and the domain $\hat{\Omega}$ is a rectangle. In terms of coordinates, matrix block and equi-dimensional and the reduced fracture geometry are given as It poses no additional difficulty in considering higher dimensions, say $\mathbb{R}^n, n = 3$ instead of $n = 2$ here. In case $n = 3$, the fracture is a two-dimensional surface. To have more generality, we can consider a non-self-intersecting one-dimensional manifold $\hat{\tau}$ with the fracture represented as

$$\hat{\Omega}_f = \{x \in \hat{\Omega} : \hat{x} = \hat{s} + \hat{\phi} n_\tau, \text{ for some } \hat{s} \in \hat{\tau} \text{ and } |\hat{\phi}| < \frac{l}{2}\}.$$

Here l is the width of the fracture at $\hat{s}$ in the normal direction, and n_τ is the outward unit normal to $\hat{\tau}$.

In this system we consider a two-phase flow in $\hat{\Omega}_m$ governed by Darcy law and the mass conservation equation where $m \in \{m_1, m_2, f\}$. Let $\hat{p}_{wm}$ denote the pressure of water phase and $\hat{p}_{om}$ the phase pressure of the oil. The saturation of water is $\hat{S}_{wm}$ and that of oil is $\hat{S}_{om}$. It holds at each point in $\hat{\Omega}$ and for all $t \in (0, T)$

$$\begin{aligned}
&\partial_t(\hat{\phi}_m \hat{S}_{wm}) + \nabla \cdot \hat{u}_{wm} = \hat{f}_{wm},\\
&\partial_t(\hat{\phi}_m \hat{S}_{om}) + \nabla \cdot \hat{u}_{om} = \hat{f}_{om},\\
&\hat{u}_{wm} = -\frac{\hat{\mathbf{K}}\hat{K}_{rw}}{\hat{\mu}_w}\nabla \hat{p}_{wm},\\
&\hat{u}_{om} = -\frac{\hat{\mathbf{K}}\hat{K}_{ro}}{\hat{\mu}_o}\nabla \hat{p}_{om}.
\end{aligned} \tag{1}$$

The first two equations are conservation of mass of water and oil phase, respectively. The next two equations are the Darcy law that describes the flux as the gradient of the respective phase pressures. The porosity is denoted by $\hat{\phi}$. The source/sink terms $\hat{f}_{im}$ on the right hand side stands for water or oil injections/outflow. Furthermore, $\hat{\mathbf{K}}$ is the absolute permeability and $\hat{K}_{rw}(\hat{S}_w)$ and $\hat{K}_{ro}(\hat{S}_o)$ denote the relative permeability of water and oil, respectively and are functions of the respective saturations. Moreover, $\hat{\mu}_w$ and $\hat{\mu}_o$ are dynamic viscosities of water and oil. For simplicity, the absolute permeability $\hat{\mathbf{K}}$ will be considered as a scalar quantity and in the matrix blocks this will be equal to 1. Extension to an anisotropic case is a straight forward. In the fracture domain the permeability is prescribed as an exponent of the fracture width ε. Here we have considered the same function $\hat{k}_{rw}$ and $\hat{k}_{ro}$ in all the three subdomains. However, considering different functions in the three subdomains possess no additional difficulty, and can be easily accommodated.

The model needs further equations for its completion. First is the saturation constraint at each point in space and time in each of the subdomains,

$$\hat{S}_{wm} + \hat{S}_{om} = 1.$$

The second is the closure condition where the capillary pressure for $m \in \{m_1, m_2, f\}$,

$$\hat{p}_{cm}(\hat{S}_{wm}) = \hat{p}_{wm} - \hat{p}_{om},$$

is a given function of saturation. We make the following assumptions on the coefficients. For $m \in \{m_1, m_2, f\}$,

1. The relative permeability $\hat{K}_{rw}, \hat{K}_{ro}$ is assumed to be strictly positive. The absolute permeability $\mathbf{K}$ is a positive tensor bounded both from above and below by strictly positive constants.
2. The capillary pressure $p_{cm} : [0,1] \mapsto \mathbb{R}$ is a positive monotonically decreasing smooth function with the $-p'_{cm} \geq \delta > 0$. Moreover, the inverse function $(p_{cm})^{-1} : \mathbb{R} \mapsto [0,1]$ exists and is assumed to be a smooth function.

In short, we are considering a non-degenerate system of equations with smooth coefficients in each subdomains. Since our approach is formal, these assumptions are needed to justify the asymptotics. To complete the description, we need to specify the boundary, interface conditions, and the initial conditions. For the sake of convenience homogeneous Dirichlet boundary conditions are considered. The interface

conditions are the continuity of the pressure and the continuity of flux. The precise equations will be written below. The initial conditions are assumed to be given $p_{wm}(t=0) = p^0_{wm}$, $p_{om}(t=0) = p^0_{om}$. Using the invertibility of the capillary pressure, this also provides the initial conditions for the saturations.

2.2. Non-dimensionalization

We define $\varepsilon := \frac{l}{L}$, that is the ratio of the fracture width to its length, and to denote that the parameters are dependent on the size of ε, we denote them with a subscript ε. Here L is the reference length scale, and the geometry is in the dimensionless form.

$$\begin{aligned} \Omega_1^\varepsilon &:= (0,1)\times(\tfrac{\varepsilon}{2}, 1+\tfrac{\varepsilon}{2}), & \Gamma_1^\varepsilon &:= (0,1)\times\{\tfrac{\varepsilon}{2}\},\\ \Omega_2^\varepsilon &:= (0,1)\times(-1-\tfrac{\varepsilon}{2}, -\tfrac{\varepsilon}{2}), & \Gamma_2^\varepsilon &:= (0,1)\times\{-\tfrac{\varepsilon}{2}\},\\ \Omega_f^\varepsilon &:= (0,1)\times(-\tfrac{\varepsilon}{2}, \tfrac{\varepsilon}{2}), & \Gamma &:= (0,1)\times\{0\}. \end{aligned} \tag{2}$$

The dimensionless pressure heads are given by $p_{m_j i} = \hat{p}_{m_j i}/L$ and $p_{f_j i} = \hat{p}_{f_j i}/L$. The dimensionless time is set as $t = \hat{t}/\bar{T}$ and the final time as $T = \hat{T}/\bar{T}$ where

$$\bar{T} := \frac{\phi_m L^2}{\hat{K}_{a,m}\bar{p}} = \frac{\phi_m L}{\hat{K}_{a,m}}. \tag{3}$$

We denote the dimensionless counterparts for $\hat{S}_{im}$, $\hat{\mathbf{K}}$, and $\hat{K}_{ri}$ as S_{im}, $\mathbf{K}$ and K_{ri}, respectively. We now substitute the Darcy law in the mass balance from model Eqs. (1), we get

$$\partial_t(\phi_i S^\varepsilon_{im}) - \nabla\cdot\left(\frac{\mathbf{K}_m K_{ri}(S^\varepsilon_{im})}{\mu_i}\nabla p^\varepsilon_{wm}\right) = f^\varepsilon_m, \quad \text{in } \Omega^\varepsilon_m, \tag{4}$$

where i denotes the phases o, w and m the matrix blocks m_1 and m_2. Further we assume that the porosity in the matrix blocks are equal,

$$\phi_1 = \phi_2, \tag{5}$$

and we would like to note the porosity and absolute hydraulic conductivity scaling in the fracture with respect to that of the surrounding matrix. As suggested we have assumed the following scaling for the porosity and hydraulic conductivity in the fracture domain

$$\frac{\phi_f}{\phi_m} \propto \varepsilon^\kappa, \quad \frac{K_{af}}{K_{an}} \propto \varepsilon^\lambda. \tag{6}$$

Here, κ and λ are scaling parameters. As earlier we use the Darcy law in the mass balance equation to get the dimensionless equation for the fracture

$$\partial_t(\varepsilon^\kappa S^\varepsilon_{if}) - \nabla\cdot\left(\frac{\varepsilon^\lambda \mathbf{K}_f K_{ri}(S^\varepsilon_{if})}{\mu_i}\nabla p^\varepsilon_{wf}\right) = f_f \quad \text{in } \Omega^\varepsilon_f. \tag{7}$$

We write down the full dimensionless model.

$$\begin{aligned} \partial_t(\phi_m S^\varepsilon_{im}) - \nabla\cdot\left(\frac{\mathbf{K}K_{ri}(S^\varepsilon_{im})}{\mu_i}\nabla p^\varepsilon_{im}\right) &= f^\varepsilon_{im}, && \text{in } \Omega^\varepsilon_m,\\ \partial_t(\varepsilon^\kappa S^\varepsilon_{if}) - \nabla\cdot\left(\frac{\varepsilon^\lambda \mathbf{K}K_{ri}(S^\varepsilon_{if})}{\mu_i}\nabla p^\varepsilon_{if}\right) &= f^\varepsilon_{if}, && \text{in } \Omega^\varepsilon_f,\\ S^\varepsilon_{wm} + S^\varepsilon_{om} &= 1, && \text{in } \Omega^\varepsilon_m \cup \Omega^\varepsilon_f,\\ p^\varepsilon_{cm}(S^\varepsilon_{wm}) &= p^\varepsilon_{wm} - p^\varepsilon_{om}, && \text{in } \Omega^\varepsilon_m \cup \Omega^\varepsilon_f,\\ p^\varepsilon_{im} &= p^\varepsilon_{if}, && \text{on } \Gamma^\varepsilon_m,\\ -\frac{\varepsilon^\lambda \mathbf{K}K_{ri}}{\mu_i}\nabla p^\varepsilon_{if}\cdot\mathbf{n} &= \frac{\mathbf{K}K_{ri}}{\mu_i}\nabla p^\varepsilon_{im}\cdot\mathbf{n}, && \text{on } \Gamma^\varepsilon_m,\\ p_{wm}(t=0) = p^0_{wm}, \text{ and } p_{om}(t=0) &= p^0_{om}, && \text{in } \Omega^\varepsilon_m \cup \Omega^\varepsilon_f. \end{aligned} \tag{8}$$

where $i = \{w, o\}$, and $m = \{m_1, m_2\}$ and in the third and fourth equations, m holds for $\{m_1, m_2, f\}$.

This problem motivates us to see if we can define different models depending on the permeability of the fracture. We can thus try to determine different types of upscaled models depending on the values of κ and λ as the fracture width $\varepsilon \to 0$. The scaling parameter κ is related to the storage capacity of the fracture, which means that for small κ ($\kappa < -1$) the fracture maintains its ability to store water as the fracture size tends to zero, and for large κ, $\kappa > 0$, the storage capacity decreases as the fracture tends to zero. The parameter λ is connected to the conductivity of the fracture. Here a small λ, (e.g., $\lambda < 0$) gives a high conductivity, flow can occur freely, while a high λ ($\lambda > 1$) will give us that the fracture will behave more as a barrier.

As seen in the above system of equations, we have considered the interface conditions where the pressures are continuous and the fluxes are equal at the fracture-matrix interface. In the case of two-phase flow, this may not hold true due to the presence of different capillary forces inside the fracture and in the matrix. The presence of entry pressure may lead to an extended pressure condition at the interface as derived in van Duijn and De Neef (1998). The difference in entry pressures causes oil trapping at the interface. Our approach can be used to derive the effective models in this case as well however, for simplicity, we disregard these difficulties.

3. Main results: Catalogue of effective models

We identify three classes of effective models. (i) Effective models I–IV that have continuous pressure across the fracture-matrix interface, (ii) Effective models V–VI that show a two-scale type behaviour, and (iii) Effective models VII–X that have fractures acting as barriers and the pressure across the fracture-matrix interface is disconnected. In case (ii), the pressure is given by a differential equation inside the fracture which is coupled to those in the matrix while in case (iii), the "fracture" acts as a barrier and accordingly has zero-flux boundary for the flow model in the matrix. We provide the effective models for a wide range of κ and λ and make brief remarks of them. The derivation of the reduced models is postponed to Section 4. In the different upscaled models we have that with $i = \{w, o\}$

$$[\vec{q}_{im}]_\Gamma = \left(\frac{\mathbf{K}_m K_{ri}(S_{im})}{\mu}\nabla p_{im_1}\right)\cdot\vec{n}_1 + \left(\frac{\mathbf{K}_m K_{ri}(S_{im})}{\mu}\nabla_x p_{im_2}\right)\cdot\vec{n}_2, \tag{9}$$

is the flux difference for water and oil respectively in the two solid matrix subdomains Ω_1 and Ω_2. Note that $\vec{n}_1 = -\vec{n}_2$, and that these vectors are normal to the fracture.

3.1. Effective model I

The first four models have continuous pressure. The first model gives us a two dimensional problem in the surrounding matrix blocks and a one dimensional problem in the fracture domain. The model for $\kappa = -1$, and $\lambda = -1$ with $i = \{w, o\}$ and $m = \{m_1, m_2\}$,

Effective model I

$$\begin{aligned} \partial_t S_{im} - \partial_x\left(\frac{\mathbf{K}_m K_{ri}(S_{im})}{\mu}\partial_x p_{im}\right) - \partial_y\left(\frac{\mathbf{K}_m K_{ri}(S_{im})}{\mu_i}\partial_y p_{im}\right) &= f_m && \text{in } \Omega_m,\\ \partial_t S_{if} - \partial_x\left(\frac{\mathbf{K}K_{ri}(S_{if})}{\mu}\partial_x p_{if}\right) &= [\vec{q}_{im}]_\Gamma && \text{on } \Gamma,\\ p_{im} &= p_{if} && \text{on } \Gamma,\\ p_{im}(0) &= p_{im,I} && \text{on } \Omega_m,\\ p_{if}(0) &= p_{if,I} && \text{on } \Gamma. \end{aligned}$$

The fracture behaves as a one-dimensional domain where $[\vec{q}_{wm}]_\Gamma$ and $[\vec{q}_{om}]_\Gamma$ are the flux difference for water and oil respectively in the two solid matrix subdomains Ω_1 and Ω_2. Here, the permeability is large enough to make the pressure inside the fracture to become y-independent. The storage term and the Darcy flow term both survive and this is taken as the most widely used model for fracture coupling.

3.2. Effective model II

In this case we have that $\kappa \in (-1, \infty)$, $\lambda = -1$. The porosity increase here with vanishing ε (vanishing fracture width) is less than linear. We

get the model: for $i = \{w, o\}$ and $m = \{m_1, m_2\}$,

Effective model II

$$\begin{aligned}
\partial_t S_{im} - \nabla \cdot \left(\frac{\mathbf{K}_m K_{ri}(S_{im})}{\mu} \nabla p_{im} \right) &= f_m && \text{in } \Omega_m, \\
-\partial_x \left(\frac{\mathbf{K}_f K_{ri}(S_{if})}{\mu} \partial_x p_{if} \right) &= [\vec{q}_{im}]_\Gamma && \text{on } \Gamma, \\
p_{im} &= p_{if} && \text{on } \Gamma, \\
p_{im}(0) &= p_{im,I} && \text{on } \Omega_m.
\end{aligned}$$

As in effective model I, we have that the permeability in the fracture is large enough to ensure that the fracture pressure equals the traces of the matrix pressures at the fracture-matrix interfaces and we get a jump in flux over the fracture. However, the porosity term is sublinear and thus vanishes in the limit as $\kappa > -1$.

3.3. Effective model III

This corresponds to the case $\kappa = -1$, $\lambda \in (-1, 1)$. We have the following effective model. For $i = \{w, o\}$ and $m = \{m_1, m_2\}$,

Effective model III

$$\begin{aligned}
\partial_t S_{im} - \nabla \cdot \left(\frac{\mathbf{K}_m K_{ri}(S_{im})}{\mu} \nabla p_{im} \right) &= f_m && \text{in } \Omega_m, \\
\partial_t (S_{if}) &= [\vec{q}_{im}]_\Gamma && \text{on } \Gamma, \\
p_{im} &= p_{if} && \text{on } \Gamma, \\
p_{im}(0) &= p_{im,I} && \text{on } \Omega_m, \\
p_{if}(0) &= p_{if,I} && \text{on } \Gamma.
\end{aligned}$$

Here, only the flux terms vanish in the limit, and the fracture is able to store and release fluids from the solid matrix. The pressure at the fracture interfaces are retained, in other words, the fracture interface conditions for Ω_1 and Ω_2 are equal to the pressure inside the fracture.

3.4. Effective model IV

This case is for $\kappa \in (-\infty, -1)$, $\lambda \in (-1, 1)$. It has been partly covered by previous cases. The pressure and the normal fluxes become continuous at the interface. In practice, the fracture has disappeared as a physical entity and can be ignored in the upscaled model.

Effective model IV

$$\begin{aligned}
\partial_t S_{im} - \nabla \cdot \left(\frac{\mathbf{K}_m K_{ri}(S_{im})}{\mu} \nabla p_{im} \right) &= f_m && \text{in } \Omega_m, \\
[\vec{q}_{im}]_\Gamma &= 0 && \text{on } \Gamma, \\
p_{im} &= p_{if} && \text{on } \Gamma, \\
p_{im}(0) &= p_{im,I} && \text{on } \Omega_m.
\end{aligned}$$

3.5. Effective model V

This is the first effective model with discontinuous pressure over the fracture. First we will consider the case where $\kappa = -1$, and $\lambda = 1$.

$$\partial_x = \partial_\xi, \quad \text{and } \partial_y = \tfrac{1}{\varepsilon} \partial_\eta. \tag{10}$$

Here we have rescaled the fracture subdomain Ω_f^ε to an ε independent subdomain Ω_f.

$$\Omega_f := (0, 1) \times (-\tfrac{1}{2}, \tfrac{1}{2}), \tag{11}$$

where the $(0, 1)$ term is the rescaling of the x coordinates now denoted as ξ, and the $(-\frac{1}{2}, \frac{1}{2})$ term is the rescaling of the y coordinates now denoted as η. Notice that the solution in the fracture in both effective models V and VI depends on η. The value $\eta = \frac{1}{2}$ corresponds to the boundary bottom boundary of Ω_{m_1} (at $y = 0+$). Similarly, $\eta = -\frac{1}{2}$ corresponds to the top boundary of Ω_{m_2} ($y = 0-$). These models will be referred to as "two-scale" "models and a typical "two-scale" model, has the scaling such that we need to resolve the details of the fracture. In this sense, representing the fracture as an interface is not fully justified. The original problem is divided into three coupled subdomains that are solved separately using boundary conditions from each other. For $i = \{w, o\}$ and $m = \{m_1, m_2\}$,

Effective model V

$$\begin{aligned}
\partial_t S_{im} - \nabla \cdot \left(\frac{\mathbf{K}_m K_{ri}(S_{im})}{\mu} \nabla p_{im} \right) &= f_m && \text{in } \Omega_m, \\
p_{im_1}(t, \xi, 0) &= p_{if}(t, \xi, \tfrac{1}{2}) && \text{for } (t, \xi) \in X^T, \\
p_{im_2}(t, \xi, 0) &= p_{if}(t, \xi, -\tfrac{1}{2}) && \text{for } (t, \xi) \in X^T, \\
p_{im}(0) &= p_{im,I} && \text{on } \Omega_m.
\end{aligned}$$

Here for each $\xi \in X$ one determines $p_{if}(\cdot, \xi, \cdot)$ as the solution to the parabolic differential equation in one dimensional spatial domain

Effective model V

$$\begin{aligned}
&\partial_t S_{if} - \partial_\eta \left(\frac{\mathbf{K}_f K_{ri}(S_{if})}{\mu} \partial_\eta p_{if} \right) = 0 \quad \text{for } (t, \eta) \in (-\tfrac{1}{2}, \tfrac{1}{2}) \times (0, T], \\
&\left(-\frac{\mathbf{K}_f K_{ri}(S_{if})}{\mu} \nabla p_{if} \right)(t, \xi, \tfrac{1}{2}) \cdot \vec{n} = \left(-\frac{\mathbf{K}_{m_1} K_{ri}(S_{im_1})}{\mu} \nabla p_{im_1} \right)(t, \xi, 0) \cdot \vec{n} \quad \text{for } t \in (0, T], \\
&\left(-\frac{\mathbf{K}_f K_{ri}(S_{if})}{\mu} \nabla p_{if} \right)(t, \xi, -\tfrac{1}{2}) \cdot \vec{n} = \left(-\frac{\mathbf{K}_{m_2} K_{ri}(S_{im_2})}{\mu} \nabla p_{im_2} \right)(t, \xi, 0) \cdot \vec{n} \quad \text{for } t \in (0, T], \\
&p_{if}(0) = p_{if,I} \quad \text{for } \eta \in (-\tfrac{1}{2}, \tfrac{1}{2}).
\end{aligned}$$

3.6. Effective model VI

The same happens for the effective model where $\kappa > -1$. The effective model remains the same as in the previous case, except for the storage term, it vanishes. For $i = \{w, o\}$ and $m = \{m_1, m_2\}$,

Effective model VI

$$\begin{aligned}
\partial_t S_{im} - \nabla \cdot \left(\frac{\mathbf{K}_m K_{ri}(S_{im})}{\mu} \nabla p_{im} \right) &= f_m && \text{in } \Omega_m, \\
p_{im_1}(t, \xi, 0) &= p_{if}(t, \xi, \tfrac{1}{2}) && \text{for } (t, \xi) \in X^T, \\
p_{im_2}(t, \xi, 0) &= p_{if}(t, \xi, -\tfrac{1}{2}) && \text{for } (t, \xi) \in X^T, \\
p_{im}(0) &= p_{im,I} && \text{on } \Omega_m.
\end{aligned}$$

For any $(t, \xi) \in X^T$, $p_{if}(t, \xi, .)$ solves the one-dimensional elliptic auxiliary problem

Effective model VI

$$\begin{aligned}
&-\partial_\eta \left(\frac{\mathbf{K}_f K_{ri}(S_{if})}{\mu} \partial_\eta p_{if} \right) = 0 \text{ for } \eta \in (-\tfrac{1}{2}, \tfrac{1}{2}), \\
&\left(-\frac{\mathbf{K}_f K_{ri}(S_{if})}{\mu} \nabla p_{if} \right)(t, \xi, \tfrac{1}{2}) \cdot \vec{n} = -\left(\frac{\mathbf{K}_{m_1} K_{ri}(S_{im_1})}{\mu} \nabla p_{im_1} \right)(t, \xi, 0) \cdot \vec{n}, \\
&\left(-\frac{\mathbf{K}_f K_{ri}(S_{if})}{\mu} \nabla p_{if} \right)(t, \xi, -\tfrac{1}{2}) \cdot \vec{n} = -\left(\frac{\mathbf{K}_{m_2} K_{ri}(S_{im_2})}{\mu} \nabla p_{im_2} \right)(t, \xi, 0) \cdot \vec{n}.
\end{aligned}$$

3.7. Effective model VII

In the case where $\lambda > 1$ and $\kappa = -1$ we get a discontinuous pressure over the fracture interface. The result is that the fracture flux is zero and it behaves as a barrier. The two domains Ω_1 and Ω_2 can be solved separately. For $i = \{w, o\}$ and $m = \{m_1, m_2\}$,

Effective model VII

$$\begin{aligned}
\partial_t S_{im} - \nabla \cdot \left(\frac{\mathbf{K}_m K_{ri}(S_{im})}{\mu} \nabla p_{im} \right) &= f_m && \text{in } \Omega_m, \\
\left(-\frac{\mathbf{K}_m K_{ri}(S_{im})}{\mu} \nabla p_{im} \right) \cdot \vec{n}_m &= 0 && \text{at } \Gamma^T, \\
p_{im}(0) &= p_{im,I} && \text{on } \Omega_m, \\
\partial_t (S_{if})(t, x, \eta) &= 0, \\
p_{if}(0) &= p_{if,I}.
\end{aligned}$$

3.8. Effective model VIII

In the case where $\lambda > 1$ and $\kappa > -1$ there is little difference from case VII. The only difference is that the storage term in the fracture drops out in the limit of $\varepsilon \to 0$. For $i = \{w, o\}$ and $m = \{m_1, m_2\}$, we end up with the model

Effective model VIII

$$\begin{aligned} \partial_t S_{im} - \nabla \cdot \left(\frac{\mathbf{K}_m K_{ri}(S_{im})}{\mu} \nabla p_{im} \right) &= f_m && \text{in } \Omega_m, \\ \left(\frac{\mathbf{K}_m K_{ri}(S_{im})}{\mu} \nabla p_{im} \right) \cdot \vec{n}_m &= 0 && \text{at } \Gamma^T, \\ p_{im}(0) &= p_{im,I} && \text{on } \Omega_m. \end{aligned}$$

3.9. Effective model IX

The two last effective models are models with spatially constant pressure in the fracture. The permeability in the fracture is so large that the pressure in the fracture will be the same short time after a pressure change. The reduced models will depend only on the time, $p_{wf}(t, y) = p_{wf}(t)$ and $p_{of}(t, y) = p_{of}(t)$. For the models this means that the fracture endpoints cannot impose different pressures at the fracture endpoints. The effective model 9 is for the cases where $\kappa = -1$ and $\lambda < -1$. One get for $i = \{w, o\}$ and $m = \{m_1, m_2\}$,

Effective model IX

$$\begin{aligned} \partial_t S_{im} - \nabla \cdot \left(\frac{\mathbf{K}_m K_{ri}(S_{im})}{\mu} \nabla p_{im} \right) &= f_m && \text{in } \Omega_m, \\ \partial_t (S_{if})(t) = \int_0^1 [\vec{q}_{im}]_\Gamma \, dx && \text{for } t \in (0, T], \\ p_{im} &= p_{if} && \text{on } \Gamma, \\ p_{im}(0) &= p_{im,I} && \text{on } \Omega_m, \\ p_{if}(0) &= p_{if,I} && \text{on } \Gamma. \end{aligned}$$

The pressure is spatially constant and continuous in the fracture and therefore, it must be spatially constant at the interfaces as well.

3.10. Effective model X

This case is for $\kappa > -1$ and $\lambda < -1$. Here the storage term vanishes. There is no equation giving the pressure in the fracture and we get for $i = \{w, o\}$ and $m = \{m_1, m_2\}$,

Effective model X

$$\begin{aligned} \partial_t S_{im} - \nabla \cdot \left(\frac{\mathbf{K}_m K_{ri}(S_{im})}{\mu} \nabla p_{im} \right) &= f_m && \text{in } \Omega_m, \\ p_{im} &= p_{if} && \text{on } \Gamma, \\ p_{im}(0) &= p_{im,I} && \text{on } \Omega_m. \end{aligned}$$

where for each t$\in$ $(0, T]$ the time-dependent function $p_{if} = p_{if}(t)$ is determined such that $\int_0^1 [\vec{q}_m]_\Gamma \, dx = 0$.

Remark 3.1. We make a brief comparison with the fracture models that are widely used in practice (see e.g., Berre et al. (2019)). We refer to Martin et al. (2005) where similar models are derived for single phase flow, and to Ahmed et al. (2017) for two-phase flow models. Our results here are different in these respects: the derivation follows different arguments and secondly, the final results are consistent in certain regimes of the parameters yet not identical.

The derivation in Martin et al. (2005) and in Ahmed et al. (2017) takes place in three steps. First, the Darcy flow equation along the fracture surface is obtained immediately by considering the flux component in the tangential direction of the fracture. Second, one integrates the flow equation along the transverse direction in the fracture subdomain. Using the continuity of fluxes at the matrix/fracture interfaces, this yields a surface equation with the jump in the matrix flux term as a source term. The third step is a closure relationship by *postulating* a pressure profile in the fracture. This is in contrast with our approach. We assume a scaling of hydraulic properties on ε and κ and use a formal asymptotic ansatz where we only consider the terms of $O(\varepsilon)$ as this is the leading term. Once the choice of scaling is made, the rest of the steps follow without any additional assumptions. In particular, our approach does not postulate any closure condition on the pressure inside the fracture as this is part of the solution. Also we mention that in the references cited, the closure condition introduces a parameter in the effective model for the fracture. Here, we have a catalogue of models and no additional parameter is necessary. Moreover, for several of the regimes considered here, the derivation is sustained by mathematically rigorous proofs (see List et al. (2020)).

In terms of the final results, we remark that for certain regimes, e.g., $\lambda = 1$, our approach yields that the fracture flow cannot be collapsed on a surface and we must resolve the details of the flow there. However, in the references and currently in practice as well, such two-scale models are not used and instead a mixed dimensional model is used irrespective of the parameter range.

Remark 3.2. This paper considers a simple geometry for the fracture embedded in a porous matrix. Besides, our model is a standard two-phase flow model with interface conditions across the matrix/fracture interface. This is consistent with our objective to illustrate the role of properties of the fracture in determining the appropriate Discrete Fracture Network (DFN) model. The two natural extensions are in the fracture networks and introducing further multiphysics. The former extension requires defining models at different scales, e.g., in the intersection of the fracture equi-dimensional subdomains. This would introduce more scales for the hydraulic properties in the intersecting subdomains and the latter corresponds to reactive multiphase flow, nonlinear interface conditions, or more general models involving thermal and mechanical models. Also, differences in the composition of fracture and matrix may cause strong heterogeneities in the constitutive relations, manifested as capillary barriers and entry pressure effects, over the fracture–matrix interface (van Duijn et al., 2007). Depending on the specific form of relative permeabilities and capillary pressure functions, these heterogeneities are known to cause numerical challenges. The formal asymptotic approach used here can be used to incorporate these difficulties. For further uses, we mention that this approach can be used to provide arguments for the mixed dimensional models proposed in Boon et al. (2017) based on physical arguments. In the same spirit, the reduced models are derived for fracture networks in Formaggia et al. (2014) building on the work of Martin et al. (2005). Our work can be used to similarly provide a hierarchy of reduced models based on the properties of the fractured networks.

4. Formal upscaling and derivation of effective models

We perform a formal upscaling for the above system of equations to derive the effective equations. For quantities in the subdomain Ω_{im}, ($i \in \{w, o\}$, $m \in \{m_1, m_2, f\}$), one makes the following ansatz for the pressure:

$$p_{im}^{\varepsilon} = p_{im0} + \varepsilon p_{im1} + O(\varepsilon^2), \tag{12}$$

and the corresponding ansatz for the saturations

$$S_{im}^{\varepsilon} = S_{im0} + \varepsilon S_{im1} + O(\varepsilon^2). \tag{13}$$

4.1. Interface conditions

Next, we treat the interface conditions. This preparation will be useful in the derivation of the effective models. We take the interface

conditions after the formal upscaling

$$\begin{aligned} p_{wf0} + \varepsilon p_{wf1} + O(\varepsilon^2) &= p_{wm_1 0} + \varepsilon p_{wm_1 1} + O(\varepsilon^2), \quad \text{on } \Gamma_1^\epsilon, \\ p_{wf0} + \varepsilon p_{wf1} + O(\varepsilon^2) &= p_{wm_2 0} + \varepsilon p_{wm_2 1} + O(\varepsilon^2), \quad \text{on } \Gamma_2^\epsilon, \\ p_{of0} + \varepsilon p_{of1} + O(\varepsilon^2) &= p_{om_1 0} + \varepsilon p_{om_1 1} + O(\varepsilon^2), \quad \text{on } \Gamma_1^\epsilon, \\ p_{of0} + \varepsilon p_{of1} + O(\varepsilon^2) &= p_{om_2 0} + \varepsilon p_{om_2 1} + O(\varepsilon^2), \quad \text{on } \Gamma_2^\epsilon, \end{aligned} \tag{14}$$

and see that the effective pressure interface conditions up to the leading order becomes

$$\begin{aligned} p_{wf0} &= p_{wm_1 0}, \quad p_{of0} = p_{om_1 0}, \quad \text{on } \Gamma, \\ p_{wf0} &= p_{wm_2 0}, \quad p_{of0} = p_{om_2 0}, \quad on \Gamma. \end{aligned} \tag{15}$$

Recalling the scaling introduced in the Effective Model 5 for ξ and η, the derivatives get transformed to

$$\partial_x \mapsto \partial_\xi \quad \text{and } \partial_y \mapsto \tfrac{1}{\epsilon}\partial_\eta.$$

and the interface conditions at Γ_1 and Γ_2 become

$$\begin{aligned} \epsilon^{\lambda-1}\frac{\mathbf{K}K_{rw}}{\mu_w}\partial_\eta p^\epsilon_{wf} &= \frac{\mathbf{K}K_{rw}}{\mu_w}\partial_y p^\epsilon_{wm_1} \quad \text{on } \Gamma, \\ \epsilon^{\lambda-1}\frac{\mathbf{K}K_{ro}}{\mu_o}\partial_\eta p^\epsilon_{of} &= \frac{\mathbf{K}K_{ro}}{\mu_o}\partial_y p^\epsilon_{om_2} \quad \text{on } \Gamma. \end{aligned} \tag{16}$$

for $j = 1, 2$.

From the interface conditions in (16), we see that when $\lambda > 1$ for an $\epsilon \to 0$ we have that the left hand side goes towards zero leading to the following interface conditions for the leading order term for the matrix subdomain fluxes

$$\begin{aligned} \frac{\mathbf{K}K_{rw}}{\mu_w}\partial_y p_{wm_1 0} &= 0 \quad \text{on } \Gamma, \\ \frac{\mathbf{K}K_{rw}}{\mu_w}\partial_y p_{wm_2 0} &= 0 \quad \text{on } \Gamma, \\ \frac{\mathbf{K}K_{ro}}{\mu_o}\partial_y p_{om_1 0} &= 0 \quad \text{on } \Gamma, \\ \frac{\mathbf{K}K_{ro}}{\mu_o}\partial_y p_{om_2 0} &= 0 \quad \text{on } \Gamma. \end{aligned} \tag{17}$$

For the case where $\lambda = 1$ the interface conditions become

$$\begin{aligned} \frac{\mathbf{K}K_{rw}}{\mu_w}\partial_\eta p_{wm_f 0} &= \frac{\mathbf{K}K_{rw}}{\mu_w}\partial_\xi p_{wm_1 0} \quad \text{on } \Gamma, \\ \frac{\mathbf{K}K_{rw}}{\mu_w}\partial_\eta p_{wm_f 0} &= \frac{\mathbf{K}K_{rw}}{\mu_w}\partial_\xi p_{wm_2 0} \quad \text{on } \Gamma, \\ \frac{\mathbf{K}K_{ro}}{\mu_o}\partial_\eta p_{om_f 0} &= \frac{\mathbf{K}K_{ro}}{\mu_o}\partial_\xi p_{om_1 0} \quad \text{on } \Gamma, \\ \frac{\mathbf{K}K_{ro}}{\mu_o}\partial_\eta p_{om_f 0} &= \frac{\mathbf{K}K_{ro}}{\mu_o}\partial_\xi p_{om_2 0} \quad \text{on } \Gamma. \end{aligned} \tag{18}$$

For $\lambda < 1$, we keep it in the same form. We also state the energy estimate for the model equations. This will allow us to conclude that the leading order terms p_{wf0}, p_{of0} are independent of y. We multiply the model Eqs. (8) by $p^\epsilon_{wm_1}$, $p^\epsilon_{om_1}$, $p^\epsilon_{wm_2}$, $p^\epsilon_{om_2}$, p^ϵ_{wf}, p^ϵ_{of} and integrate over the respective domains Ω^ϵ_f, Ω^ϵ_1 and Ω^ϵ_2. Using the Gauss divergence theorem to transfer the div to the other term and using the boundary condition, we obtain

$$\begin{aligned} &\int_{\Omega^\epsilon_f} \epsilon^\kappa \partial_t S^\epsilon_{of}(p^\epsilon_{of} - p^\epsilon_{wf})dx + \epsilon^\lambda \int_{\Omega^\epsilon_f} KK_{rw}(S^\epsilon_{wf})\left|\nabla p^\epsilon_{wf}\right|^2 dx \\ &+ \epsilon^\lambda \int_{\Omega^\epsilon_f} KK_{ro}(S^\epsilon_{of})\left|\nabla p^\epsilon_{of}\right|^2 dx + \\ &+ \int_{\Omega^\epsilon_1} KK_{ro}(S^\epsilon_{om_1})\left|\nabla p^\epsilon_{om_1}\right|^2 dx \\ &+ \int_{\Omega^\epsilon_1} KK_{rw}(S^\epsilon_{wm_1})\left|\nabla p^\epsilon_{wm_1}\right|^2 dx + \int_{\Omega^\epsilon_2} KK_{rw}(S^\epsilon_{wm_2})\left|\nabla p^\epsilon_{wm_2}\right|^2 dx \\ &+ \int_{\Omega^\epsilon_2} KK_{ro}(S^\epsilon_{om_2})\left|\nabla p^\epsilon_{om_2}\right|^2 dx + \int_{\Omega^\epsilon_1} \partial_t S^\epsilon_{om_1}(p^\epsilon_{om_1} - p^\epsilon_{wm_1})dx \\ &+ \int_{\Omega^\epsilon_2} \partial_t S^\epsilon_{om_2}(p^\epsilon_{om_2} - p^\epsilon_{wm_2})dx = 0. \end{aligned}$$

Integrating over time from 0 to an arbitrary time t, we obtain

$$\begin{aligned} &\epsilon^\kappa \int_{\Omega^\epsilon_f} B(S^\epsilon_{wf}(t)) + \epsilon^\lambda \int_0^t \int_{\Omega^\epsilon_f} KK_{rw}(S^\epsilon_{wf})\left|\nabla p^\epsilon_{wf}\right|^2 dxdt \\ &+ \epsilon^\lambda \int_0^t \int_{\Omega^\epsilon_f} KK_{ro}(S^\epsilon_{of})\left|\nabla p^\epsilon_{of}\right|^2 dxdt + \int_0^t \int_{\Omega^\epsilon_1} KK_{ro}(S^\epsilon_{om_1})\left|\nabla p^\epsilon_{om_1}\right|^2 dxdt \\ &+ \int_0^t \int_{\Omega^\epsilon_1} KK_{rw}(S^\epsilon_{wm_1})\left|\nabla p^\epsilon_{wm_1}\right|^2 dxdt + \int_0^t \int_{\Omega^\epsilon_2} KK_{rw}(S^\epsilon_{wm_2})\left|\nabla p^\epsilon_{wm_2}\right|^2 dxdt \\ &+ \int_0^t \int_{\Omega^\epsilon_2} KK_{ro}(S^\epsilon_{om_2})\left|\nabla p^\epsilon_{om_2}\right|^2 dxdt \int_{\Omega^\epsilon_1} B(S^\epsilon_{wm_1}(t)) + \int_{\Omega^\epsilon_f} B(S^\epsilon_{wm_2}(t)) \le C. \end{aligned}$$

Here,

$$B(z) = \int_0^z P_c(\tilde{z})d\tilde{z},$$

and is a positive quantity. In the transformed co-ordinates $\xi = x, \eta = y/\epsilon$ inside the fracture region, we get

$$\begin{aligned} &\frac{\epsilon^{\lambda+1}}{\epsilon^2}\int_0^t \int_{-1/2}^{1/2} KK_{rw}(S^\epsilon_{wf})\left|\partial_\eta p^\epsilon_{wf}\right|^2 d\eta dt \\ &+ \epsilon^\lambda \int_0^t \int_0^1 KK_{rw}(S^\epsilon_{wf})\left|\partial_\xi p^\epsilon_{wf}\right|^2 d\xi dt \le C. \end{aligned}$$

Using non-degeneracy of K_{rw},

$$\partial_\eta p^\epsilon_{wf} \le C\epsilon^{1-\lambda}.$$

This allows us to conclude that the leading order term p_{wf0} in the expansion of p^ϵ_{wf}, for $\lambda < 1$, is independent of the $y-$ co-ordinate as well as the η co-ordinate in the re-scaled variables. That is,

$$p_{wf0} = p_{wf0}(x). \tag{19}$$

This implies that for $\lambda < 1$, the leading order approximation for the water pressure in the fracture is independent of the y direction. The same conclusion holds for oil pressure. Thus, for $\lambda < 1$, we have

$$p_{of0} = p_{of0}(x). \tag{20}$$

This completes the preparation for deriving the effective equations. Now we consider the model equations for different regimes for κ and λ.

4.2. Derivation of the effective models

We begin with the matrix subdomain equations. The upscaling here proceeds without much difficulty.

4.2.1. Matrix subdomains

Recall the model equation in the matrix subdomain for $i = \{w, o\}$, $m = \{m_1, m_2\}$

$$\partial_t(\phi_m S_{im}) - \nabla \cdot \left(\frac{\mathbf{K}K_{ri}(S_{im})}{\mu_i}\nabla p_{im}\right) = f_{im} \quad \text{in } \Omega^\epsilon_m.$$

Note that in the matrix subdomain, the derivatives do not introduce any ϵ and it gets introduced only in the expansion of the variables. Substituting the ansatz for pressure and saturation, we obtain up to $O(\epsilon^2)$ approximation,

$$\begin{aligned} &\partial_t(\phi_m(S_{im0} + \epsilon S_{im1})) - \nabla \cdot \left(\frac{\mathbf{K}K_{ri}(S_{im0} + \epsilon S_{im1})}{\mu_i}\nabla(p_{im0} + \epsilon p_{im1})\right) \\ &= f_{im} \quad \text{in } \Omega^\epsilon_m. \end{aligned}$$

Restricting up to leading order, we have that Ω^ϵ_m tends to Ω_m as ϵ tends to zero,

$$\partial_t(\phi_m S_{im0}) - \nabla \cdot \left(\frac{\mathbf{K}K_{ri}(S_{im0})}{\mu_i}\nabla p_{im0}\right) = f_{im} \quad \text{in } \Omega_m.$$

This reflects the stability of the matrix subdomains with respect to the upscaling. This is expected since the matrix subdomain converges uniformly to $\epsilon-$ independent subdomain and the coefficients are $\epsilon-$ independent. This holds true regardless of the value of λ and κ.

4.2.2. Fracture subdomain

Next, we consider the fracture equation.

$$\partial_t(\varepsilon^\kappa S_{if}) - \nabla\cdot\left(\frac{\varepsilon^\lambda \mathbf{K}K_{rw}(S_{if})}{\mu_i}\nabla p_{if}\right) = f_{if} \quad \text{in } \Omega_f^\varepsilon, \tag{21}$$

and with the rescaling of the fracture domain, the rescaled equations in the Ω_f become

$$\begin{aligned}
&\partial_t(\varepsilon^\kappa(S_{wf0}+\varepsilon S_{wf1})) + \tfrac{1}{\varepsilon^2}\partial_\eta\left(-\frac{\varepsilon^\lambda \mathbf{K}K_{rw}(S_{wf0}+\varepsilon S_{wf1})}{\mu_w}\partial_\eta(p_{wf0}+\varepsilon p_{wf1})\right)\\
&+\partial_\xi\left(-\frac{\varepsilon^\lambda \mathbf{K}K_{rw}(S_{wf0}+\varepsilon S_{wf1})}{\mu_w}\partial_\xi(p_{wf0}+\varepsilon p_{wf1})\right) = f_{wf},\\
&\partial_t(\varepsilon^\kappa(S_{of0}+\varepsilon S_{of1})) + \tfrac{1}{\varepsilon^2}\partial_\eta\left(-\frac{\varepsilon^\lambda \mathbf{K}K_{ro}(S_{of0}+\varepsilon S_{of1})}{\mu_o}\partial_\eta(p_{of0}+\varepsilon p_{of1})\right)\\
&+\partial_\xi\left(-\frac{\varepsilon^\lambda \mathbf{K}K_{ro}(S_{of0}+\varepsilon S_{of1})}{\mu_o}\partial_\xi(p_{of0}+\varepsilon p_{fo1})\right) = f_{of}.
\end{aligned} \tag{22}$$

4.2.3. Subcases when $\lambda < 1$

Recall that in this case p_{wf0} and p_{of0} are independent of η. By virtue of this, we conclude that $p_c(S_{w0}) = p_{of0} - p_{wf0}$ is independent of η. From the invertibility of p_c, we get that S_{wf0} is independent of η as well. Due to the saturation constraint, S_{of0} is also independent of η.

We begin with the case $\kappa = -1, \lambda = -1$. Integrating Eq. (22) over $\eta = -\frac{1}{2}$ to $\frac{1}{2}$ and multiplying the equation by ε we have

$$\begin{aligned}
&\varepsilon^{1+\kappa}\int_{-1/2}^{1/2}\partial_t(S_{wf0}+\varepsilon S_{wf1})d\eta\\
&\quad+\tfrac{1}{\varepsilon}\int_{-1/2}^{1/2}\partial_\eta\left(-\frac{\varepsilon^\lambda \mathbf{K}K_{rw}(S_{wf0}+\varepsilon S_{wf1})}{\mu_w}\partial_\eta(p_{wf0}+\varepsilon p_{wf1})\right)d\eta\\
&\quad+\varepsilon\int_{-1/2}^{1/2}\partial_\xi\left(-\frac{\varepsilon^\lambda \mathbf{K}K_{rw}(S_{wf0}+\varepsilon S_{wf1})}{\mu_w}\partial_\xi(p_{wf0}+\varepsilon p_{wf1})\right)d\eta\\
&\quad=\int_{-1/2}^{1/2}\varepsilon f_{wf}d\eta,\\
&\varepsilon^{1+\kappa}\int_{-1/2}^{1/2}\partial_t(S_{of0}+\varepsilon S_{of1})d\eta\\
&\quad+\tfrac{1}{\varepsilon}\int_{-1/2}^{1/2}\partial_\eta\left(-\frac{\varepsilon^\lambda \mathbf{K}K_{ro}(S_{of0}+\varepsilon S_{of1})}{\mu_o}\partial_\eta(p_{of0}+\varepsilon p_{of1})\right)d\eta\\
&\quad+\varepsilon\int_{-1/2}^{1/2}\partial_\xi\left(-\frac{\varepsilon^\lambda \mathbf{K}K_{ro}(S_{of0}+\varepsilon S_{of1})}{\mu_o}\partial_\xi(p_{of0}+\varepsilon p_{fo1})\right)d\eta\\
&\quad=\int_{-1/2}^{1/2}\varepsilon f_{of}d\eta.
\end{aligned}$$

The reason for multiplying by ε is obvious: this matches the scale of ε in the flux interface conditions (16). We take the leading order term and use the independence of these leading order terms $p_{wf0}, p_{of0}, S_{wf0}, S_{of0}$ of η. Moreover, the scaled right hand side is assumed to be independent of η. With these considerations,

$$\begin{aligned}
&\varepsilon^{\kappa+1}\partial_t S_{wf0} + \varepsilon^{\lambda-1}\left(-\frac{\mathbf{K}K_{rw}(S_{wf0})}{\mu_w}\partial_\eta(p_{wf0})\right)_{\eta=\frac{1}{2}}\\
&-\varepsilon^{\lambda-1}\left(-\frac{\mathbf{K}K_{rw}(S_{wf0})}{\mu_w}\partial_\eta(p_{wf0})\right)_{\eta=-\frac{1}{2}}\\
&+\varepsilon^{\lambda+1}\partial_\xi\left(-\frac{\mathbf{K}K_{rw}(S_{wf0})}{\mu_w}\partial_\xi(p_{wf0})\right) = \varepsilon f_{wf},\\
&\varepsilon^{\kappa+1}\partial_t S_{of0} + \varepsilon^{\lambda-1}\left(-\frac{\mathbf{K}K_{ro}(S_{of0})}{\mu_o}\partial_\eta(p_{of0})\right)_{\eta=\frac{1}{2}}\\
&-\varepsilon^{\lambda-1}\left(-\frac{\mathbf{K}K_{ro}(S_{of0})}{\mu_o}\partial_\eta(p_{of0})\right)_{\eta=-\frac{1}{2}}\\
&+\varepsilon^{\lambda+1}\partial_\xi\left(-\frac{\mathbf{K}K_{ro}(S_{of0})}{\mu_o}\partial_\xi(p_{of0})\right) = \varepsilon f_{of}.
\end{aligned}$$

Using the interface condition for the flux in (16) and restricting up to the leading order term.

$$\begin{aligned}
\varepsilon^{\lambda-1}\left(-\frac{\mathbf{K}K_{rw}(S_{wf0})}{\mu_w}\partial_\eta(p_{wf0})\right)_{\eta=\frac{1}{2}} &= \left(\frac{\mathbf{K}K_{rw}}{\mu_w}\partial_y p_{wm_1 0}\right)_{y=0^+},\\
\varepsilon^{\lambda-1}\left(-\frac{\mathbf{K}K_{rw}(S_{wf0})}{\mu_w}\partial_\eta(p_{wf0})\right)_{\eta=-\frac{1}{2}} &= \left(\frac{\mathbf{K}K_{rw}}{\mu_w}\partial_y p_{wm_2 0}\right)_{y=0^-}.
\end{aligned}$$

For the oil flux we get a similar expression:

$$\begin{aligned}
\varepsilon^{\lambda-1}\left(-\frac{\mathbf{K}K_{ro}(S_{of0})}{\mu_o}\partial_\eta(p_{of0})\right)_{\eta=\frac{1}{2}} &= \left(\frac{\mathbf{K}K_{ro}}{\mu_o}\partial_y p_{om_1 0}\right)_{y=0^+},\\
\varepsilon^{\lambda-1}\left(-\frac{\mathbf{K}K_{ro}(S_{of0})}{\mu_o}\partial_\eta(p_{of0})\right)_{\eta=-\frac{1}{2}} &= \left(\frac{\mathbf{K}K_{ro}}{\mu_o}\partial_y p_{om_2 0}\right)_{y=0^-}.
\end{aligned}$$

Defining the jump in the flux for the water and the oil across the fracture surface:

$$\begin{aligned}
[q_{w0}] &= \left(\frac{\mathbf{K}K_{rw}}{\mu_w}\partial_y p_{w0}\right)_{y=0^+} - \left(\frac{\mathbf{K}K_{rw}}{\mu_w}\partial_y p_{w0}\right)_{y=0^-},\\
[q_{o0}] &= \left(\frac{\mathbf{K}K_{ro}}{\mu_o}\partial_y p_{o0}\right)_{y=0^+} - \left(\frac{\mathbf{K}K_{ro}}{\mu_o}\partial_y p_{o0}\right)_{y=0^-}.
\end{aligned}$$

With these definitions for the jump in the flux on hand, we rewrite the averaged model as

$$\begin{aligned}
\varepsilon^{\kappa+1}\partial_t S_{wf0} + \varepsilon^{\lambda+1}\partial_\xi\left(-\frac{\mathbf{K}K_{rw}(S_{wf0})}{\mu_w}\partial_\xi(p_{wf0})\right) &= [q_{w0}] + f_{wf},\\
\varepsilon^{\kappa+1}\partial_t S_{of0} + \varepsilon^{\lambda+1}\partial_\xi\left(-\frac{\mathbf{K}K_{ro}(S_{of0})}{\mu_o}\partial_\xi(p_{of0})\right) &= [q_{o0}] + f_{of}.
\end{aligned} \tag{23}$$

Now in (23), we consider the different regimes of coefficients. For $\kappa = -1, \lambda = -1$, we get

$$\begin{aligned}
\partial_t S_{wf0} + \partial_\xi\left(-\frac{\mathbf{K}K_{rw}(S_{wf0})}{\mu_w}\partial_\xi(p_{wf0})\right) &= [q_{w0}] + f_{wf},\\
\partial_t S_{of0} + \partial_\xi\left(-\frac{\mathbf{K}K_{ro}(S_{of0})}{\mu_o}\partial_\xi(p_{of0})\right) &= [q_{o0}] + f_{of}.
\end{aligned} \tag{24}$$

Next we consider the case when $\kappa \in (-1, \infty)$, $\lambda = -1$. The only change from the above derivation is the storage term. This term vanishes in the limit as ε goes to zero. Indeed, for $\kappa \in (-1, \infty)$, we have

$$\varepsilon^{\kappa+1}\partial_t S_{wf0} \to 0$$

and

$$\varepsilon^{\kappa+1}\partial_t S_{of0} \to 0$$

as $\varepsilon \to 0$. With the storage term vanishing, on Γ for the coefficients $\kappa \in (-1, \infty), \lambda = -1$, it holds

$$\begin{aligned}
\partial_\xi\left(-\frac{\mathbf{K}K_{rw}(S_{wf0})}{\mu_w}\partial_\xi(p_{wf0})\right) &= [q_{w0}] + f_{wf},\\
\partial_\xi\left(-\frac{\mathbf{K}K_{ro}(S_{of0})}{\mu_o}\partial_\xi(p_{of0})\right) &= [q_{o0}] + f_{of}.
\end{aligned} \tag{25}$$

In the case when $\lambda \in (-1, 1)$ on the fracture surface Γ, we have that

$$\varepsilon^{\lambda+1}\partial_x\left(\frac{KK_{wf}}{\mu_w}\partial_x p_{wf0}\right) \to 0$$

as $\varepsilon \to 0$. The averaged equation therefore takes the form of an ODE since the flux term now drops out. On Γ it holds that

$$\begin{aligned}
\partial_t S_{wf0} &= [q_{w0}] + f_{wf},\\
\partial_t S_{of0} &= [q_{o0}] + f_{of}.
\end{aligned}$$

The next effective model is for $\kappa \in (-1, \infty)$, $\lambda \in (-1, 1)$. Partly, these intervals have been covered in the previous cases. For $\lambda \in (-1, 1)$ the flux term drops out and for $\kappa \in (-1, \infty)$, the storage term vanishes. The resulting equation therefore takes the form:

$$[q_{w0}] + f_{wf} = 0,$$

$[q_{o0}] + f_{of} = 0.$

In the absence of any source term, this case shows that the pressure is continuous over the fracture. The effective model behaves as if the fracture as a physical entity has disappeared.

4.2.4. Subcases when $\lambda = 1$

This is the critical case of λ being exactly equal to 1. In contrast to the previous case when $\lambda < 1$ led to the continuity of pressures across the fracture interface, this case leads to a discontinuous pressure. However, the pressures at the two sides of the fracture interfaces are not independent, rather they are coupled through a differential equation inside the rescaled fracture subdomain. We have different interface conditions on the two sides of the fracture, and we define the interfaces as $\Gamma_1 = \partial\Omega_1 \cap \partial\Omega_f$ and $\Gamma_2 = \partial\Omega_2 \cap \partial\Omega_f$. Let us first derive the model equations for this case before discussing more on their structures. The next case, the fifth case, is for $\kappa = -1$ and $\lambda = 1$ and we have these interface conditions

$$\begin{aligned}
-\frac{\mathbf{K}K_{rw}}{\mu_w}\partial_\eta p_{wf0} &= \frac{\mathbf{K}K_{rw}}{\mu_w}\partial_y p_{wm_1 0} \quad \text{on } \Gamma_1,\\
-\frac{\mathbf{K}K_{rw}}{\mu_w}\partial_\eta p_{wf0} &= \frac{\mathbf{K}K_{rw}}{\mu_w}\partial_y p_{wm_2 0} \quad \text{on } \Gamma_2,\\
-\frac{\mathbf{K}K_{ro}}{\mu_o}\partial_\eta p_{of0} &= \frac{\mathbf{K}K_{ro}}{\mu_o}\partial_y p_{om_1 0} \quad \text{on } \Gamma_1,\\
-\frac{\mathbf{K}K_{ro}}{\mu_o}\partial_\eta p_{of0} &= \frac{\mathbf{K}K_{ro}}{\mu_o}\partial_y p_{om_2 0} \quad \text{on } \Gamma_2
\end{aligned} \tag{26}$$

and the continuity of the pressure

$$\begin{aligned}
&p_{wf0}(t,x,\eta=-\tfrac{1}{2}) = p_{wm_1 0}(t,x,0), \quad p_{wf0}(t,x,\eta=\tfrac{1}{2}) = p_{wm_2 0}(t,x,0),\\
&p_{of0}(t,x,\eta=-\tfrac{1}{2}) = p_{om_1 0}(t,x,0), \quad p_{of0}(t,x,\eta=\tfrac{1}{2}) = p_{om_2 0}(t,x,0).
\end{aligned} \tag{27}$$

We begin again from (22). For $\lambda = 1$ and again multiplying the equation by ε and restricting up to leading order terms,

$$\begin{aligned}
&\varepsilon^{\kappa+1}\partial_t S_{wf0} + \partial_\eta\left(-\frac{\mathbf{K}K_{rw}(S_{wf0})}{\mu_w}\partial_\eta(p_{wf0})\right)\\
&\quad + \varepsilon^2\partial_\xi\left(-\frac{\mathbf{K}K_{rw}(S_{wf0})}{\mu_w}\partial_\xi(p_{wf0})\right) = \varepsilon f_{wf},\\
&\varepsilon^{\kappa+1}\partial_t S_{of0} + \partial_\eta\left(-\frac{\mathbf{K}K_{ro}(S_{of0})}{\mu_o}\partial_\eta(p_{of0})\right)\\
&\quad + \varepsilon^2\partial_\xi\left(-\frac{\mathbf{K}K_{ro}(S_{of0})}{\mu_o}\partial_\xi(p_{of0})\right) = \varepsilon f_{of}.
\end{aligned}$$

Clearly,

$$\varepsilon^2\partial_\xi\left(-\frac{\mathbf{K}K_{rw}(S_{wf0})}{\mu_w}\partial_\xi(p_{wf0})\right) \to 0, \varepsilon^2\partial_\xi\left(-\frac{\mathbf{K}K_{ro}(S_{of0})}{\mu_o}\partial_\xi(p_{of0})\right) \to 0,$$

as well as the source term goes to zero as ε vanishes. With these considerations, we obtain the following model

$$\begin{aligned}
&\varepsilon^{\kappa+1}\partial_t S_{wf0} + \partial_\eta\left(-\frac{\mathbf{K}K_{rw}(S_{wf0})}{\mu_w}\partial_\eta(p_{wf0})\right) = 0,\\
&\varepsilon^{\kappa+1}\partial_t S_{of0} + \partial_\eta\left(-\frac{\mathbf{K}K_{ro}(S_{of0})}{\mu_o}\partial_\eta(p_{of0})\right) = 0.
\end{aligned}$$

Now we consider a different regime. For $\kappa = -1$, we obtain the effective model V. The fracture flow model is given as follows

$$\begin{aligned}
&\partial_t S_{wf0} - \partial_\eta\left(\frac{\mathbf{K}K_{rw}(S_{wf0})}{\mu_w}\partial_\eta p_{wf0}\right) = 0\\
&\quad \text{for } \eta \in (-\frac{1}{2},\frac{1}{2}), (t,x) \in (0,T)\times\Gamma,\\
&\partial_t S_{of0} - \partial_\eta\left(\frac{\mathbf{K}K_{ro}(S_{of0})}{\mu_o}\partial_\eta p_{of0}\right) = 0\\
&\quad \text{for } \eta \in (-\frac{1}{2},\frac{1}{2}), (t,x) \in (0,T)\times\Gamma.
\end{aligned} \tag{28}$$

The interface conditions and the subdomain equations complete the model derivation.

Next case we treat is the case where $\kappa = (-1,\infty), \lambda = 1$. This case is almost equal to the previous case, however, the scaling of κ in the storage term is different. The interface condition remains the same. For this range of κ, the storage term vanishes in the limit as ε goes to zero. That is,

$$\varepsilon^{\kappa+1}\partial_t S_{wf0} \to 0, \quad \varepsilon^{\kappa+1}\partial_t S_{of0} \to 0.$$

The fracture equations then take the form

$$\begin{aligned}
-\partial_\eta\left(\frac{\mathbf{K}K_{rw}(S_{wf0})}{\mu_w}\partial_\eta p_{wf0}\right) = 0 \quad &\text{for } \eta \in (-\tfrac{1}{2},\tfrac{1}{2}), (t,x) \in (0,T)\times\Gamma,\\
-\partial_\eta\left(\frac{\mathbf{K}K_{ro}(S_{of0})}{\mu_o}\partial_\eta p_{of0}\right) = 0 \quad &\text{for } \eta \in (-\tfrac{1}{2},\tfrac{1}{2}), (t,x) \in (0,T)\times\Gamma.
\end{aligned} \tag{29}$$

Together with the interface conditions (26) and (27) and retaining the subdomain equation, this completes the derivation of the Effective model VI. The dependency of p_{of0}, and p_{wf0} on t and y happens via the interface conditions. Notice that in the effective models V and VI, the fracture model does not collapse into reduced dimensional fracture models and one needs to solve differential equations inside the fracture subdomain. This is what we will refer to as the two-scaled models similar to a cell problem in homogenization. This is different from what happened in the effective models I–IV where one needs to solve differential equations on the fracture surface.

4.2.5. Subcases when $\lambda > 1$

For the last two models, the permeability in the fracture is sufficiently low such that the fracture acts as a barrier. These cases are for $\kappa = -1$, $\lambda \in (1,\infty)$ and $\kappa \in (-1,\infty)$, $\lambda \in (1,\infty)$. The difference between these two cases is the scaling of the storage term, and as we have seen before, the storage term will not survive in the latter case. The subdomain equations remain unchanged as before. We then recall the interface conditions in (17) to deduce the boundary conditions for the matrix subdomain,

$$\begin{aligned}
\tfrac{\mathbf{K}K_{rw}}{\mu_w}\nabla p^\varepsilon_{wm_1 0}\cdot\mathbf{n} = 0 \quad &\text{on } \Gamma,\\
\tfrac{\mathbf{K}K_{ro}}{\mu_o}\nabla p^\varepsilon_{om_1 0}\cdot\mathbf{n} = 0 \quad &\text{on } \Gamma,\\
\tfrac{\mathbf{K}K_{rw}}{\mu_w}\nabla p^\varepsilon_{wm_2 0}\cdot\mathbf{n} = 0 \quad &\text{on } \Gamma,\\
\tfrac{\mathbf{K}K_{ro}}{\mu_o}\nabla p^\varepsilon_{om_2 0}\cdot\mathbf{n} = 0 \quad &\text{on } \Gamma.
\end{aligned} \tag{30}$$

The zero-flux boundary condition between the matrix sub domains leads to a set of subdomains that are independent of each other, and can be solved separately. The fracture equation becomes irrelevant. However, for the case when $\kappa = -1$, we can still evaluate the fracture equation by solving the differential equations,

$$\begin{aligned}
&\partial_t S_{wf0}(t,\eta,x) = 0 \quad \text{for } \eta \in (-\tfrac{1}{2},\tfrac{1}{2}), (t,x) \in (0,T)\times\Gamma,\\
&\partial_t S_{of0}(t,\eta,x) = 0 \quad \text{for } \eta \in (-\tfrac{1}{2},\tfrac{1}{2}), (t,x) \in (0,T)\times\Gamma,
\end{aligned} \tag{31}$$

as the flux terms in the fracture drop out. In the case when $\kappa \in (-1,\infty)$, $\lambda \in (1,\infty)$ even the storage term drops out making the fracture equation irrelevant. Together with retaining the initial condition and the boundary conditions, we recover the Effective models VII and VIII.

For the last two effective models, IX and X, we have the cases $\kappa = -1$, $\lambda \in (-\infty,-1)$ and $\kappa \in (-1,\infty)$, $\lambda \in (-\infty,-1)$, respectively. The permeability in this case is large enough so that the pressure becomes independent of y. Clearly in this regime, the pressures are independent of y, since λ is less than 1 as seen before. However, in this regime, the pressure also becomes independent of x. This implies that the pressure is constant along the fracture surface. This is possible only when the boundary conditions are compatible. The difference between IX and

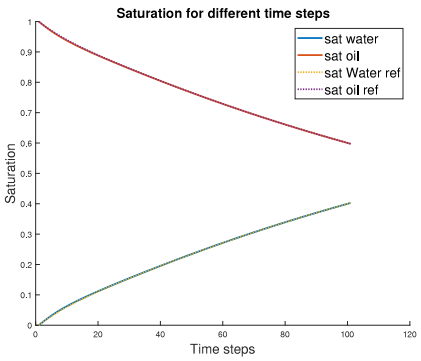

(a) Water and oil saturation in domain using $\lambda = -2$ and $\kappa = -1$.

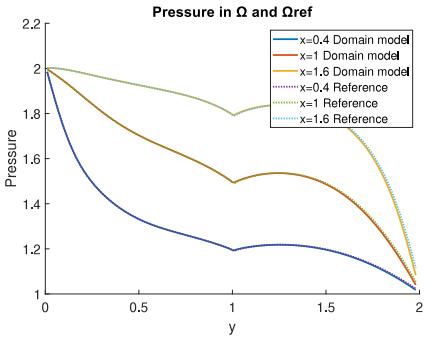

(b) Pressure in domain using using $\lambda = -2$ and $\kappa = -1$.

Fig. 2. Saturation for the whole domain and the reference model where we use Effective model I for the case when $\lambda = -2$ and $\kappa = -1$ (left) and pressure for the domain at fixed x-values for the same values of κ and λ (right). The saturations and pressures are compared to the reference solution in dotted lines.

X is that in case IX when $\kappa = -1$ the storage term survives, and the fracture pressure only depends on t. In X the storage term also drops out.

4.3. Summary of the effective models

Below we summarize the range of parameters and their corresponding effective models.

$\kappa = -1, \quad \lambda = -1$: Effective model I
$\kappa \in (-1, \infty), \lambda = -1$: Effective model II
$\kappa = -1, \quad \lambda \in (-1, 1)$: Effective model III
$\kappa \in (-1, \infty), \lambda \in (-1, 1)$: Effective model IV
$\kappa = -1, \quad \lambda = 1$: Effective model V
$\kappa \in (-1, \infty), \lambda = 1$: Effective model VI
$\kappa - 1, \quad \lambda \in (-1, -\infty)$: Effective model VII
$\kappa \in (-1, \infty), \lambda \in (-1, -\infty)$: Effective model VIII
$\kappa = -1, \quad \lambda \in (1, \infty)$: Effective model IX
$\kappa \in (-1, \infty), \lambda \in (-\infty, -1)$: Effective model X

5. Numerical examples

In this section we will numerically verify the above upscaling results. To perform numerical experiments, we use a fully implicit two-phase oil and water model as implemented in the MATLAB Reservoir Simulation Toolbox (MRST) (Lie, 2019). We use the standard finite volume scheme using two-point flux scheme (TPFA) on a static, uniform grid with rectangular cells. The geometry is built up by two smaller rectangular domains separated by a fracture as considered in the derivation. The two domains Ω_1 and Ω_2 consist of 100×50 grid blocks each. The fracture is treated in different ways depending on the effective model in use. The reference solution is obtained by solving the two-phase flow model (1) in $\Omega^\epsilon = \Omega_1^\epsilon \cup \Omega_f^\epsilon \cup \Omega_2^\epsilon$ as shown in Fig. 1. Here the fracture is solved together with the surrounding matrix using the TPFA. The domain Ω is fully saturated with oil at $t = 0$. The global pressure for the boundary conditions are taken to be of Dirichlet type on all sides with a pressure of $p = 2$ at the bottom and at the left side of the domain. On the top and right hand side the pressure is $p = 1$. At the time t=0, we have that the whole domain Ω is fully oil-saturated, and then we start the water injection. This is done by setting the saturation of the fluxes at the boundaries as water only. In our reference model we solve the full model using these boundary conditions on all the sides. However, for the upscaled models we need some interface conditions at the fracture interface. These conditions vary depending on the different effective models we use, and the different models vary depending on the values of λ and κ. The easiest case however, is the case where the fracture completely separates the two sub-domains Ω_1 and Ω_2 from each other. Here we can put a zero-flux interface condition and just solve the two sub domains Ω_1 and Ω_2 separately. We provide further information on solving each of the three effective models in the numerical tests below. The capillary pressure is implemented with a simple linear relationship of the form $p_c(S) = C(1 - S)$ which is implemented in MRST where C is a constant and S is the saturation. In the following simulations, $C = 0.01$. We do also have linear relative permeabilities for each phase.

Our approach for the validation is as follows. We select certain values of $\epsilon, \kappa, \lambda$ which determine the reference geometry and the permeabilities. We compute the pressure for the full reference model resolving the fracture thickness, i.e. we solve the equations in (8) with a finite value of ϵ and use this for our reference solution. Depending on the κ and λ we pick a suitable upscaled model from the catalogue for these values. The solution from the upscaled model is then compared to those from the reference model.

We choose three sets of representative values for κ and λ. We choose (i) $\lambda = -2, \kappa = -1$, (ii) $\lambda = 1, \kappa = -1$, and (iii) $\lambda = 2, \kappa = -1$. These three regimes correspond to permeability being quite large, critical case, and sufficiently low permeability to act as a barrier case, respectively. For these three cases, we choose three representative upscaled models from the catalogue. The three models are selected such that they are the appropriate models for the above three cases. The first model is the effective model I which has the model equations collapsed on a surface with the jump in the flux from the matrix appearing on the right hand side. The second representative model is the two-scale model, effective model V, which retains the storage term (time derivative term of saturation). The effective model VII is chosen from the class that caters to sufficiently low permeability so that the fracture acts as a barrier. Effective model I is the appropriate model for case (i) $\lambda = -2, \kappa = -1$, whereas models V and VII are appropriate for (ii) $\lambda = 1, \kappa = -1$, and (iii) $\lambda = 2, \kappa = -1$ cases, respectively.

The motivation for setting up these numerical tests is the following. For a certain parameter range, we find that the corresponding model from the catalogue is the appropriate one and matches the reference solution quite closely. Moreover, if we choose one particular model but then choose the parameters far from their range of validity, the accuracy decreases. This shows that relying on only one of these models would not be appropriate for all the range of the parameters.

5.1. Effective model I

We study the effective model I and its quality in solving the models for the three cases as mentioned above. Note that this is a mixed

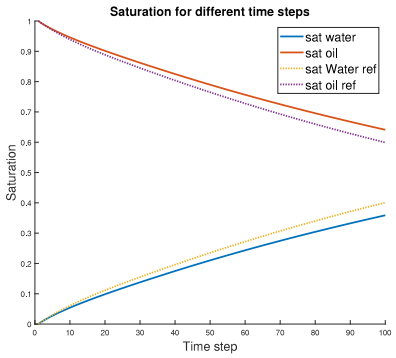

(a) Water and oil saturation in domain for the $\kappa = -1$. case where $\lambda = -2$ and $\kappa = -1$.

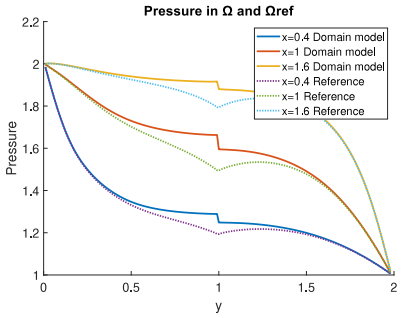

(b) Pressure in domain using using $\lambda = -2$ and

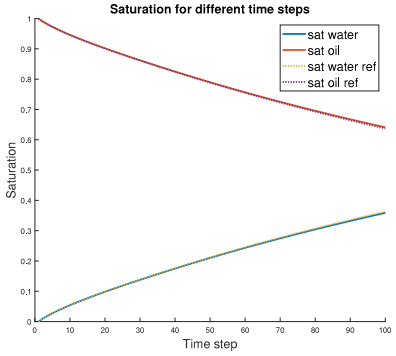

(c) Water and oil saturation in domain for the $\kappa = -1$. case where $\lambda = 1$ and $\kappa = -1$

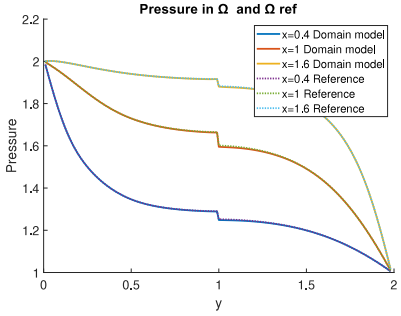

(d) Pressure in domain using using $\lambda = 1$ and

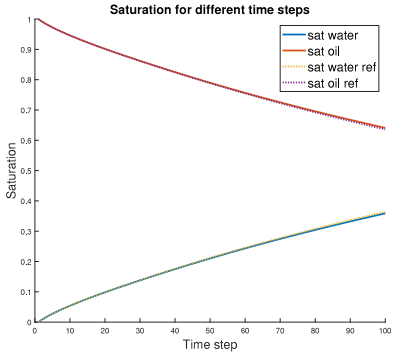

(e) Water and oil saturation in domain for the $\kappa = -1$. case where $\lambda = 2$ and $\kappa = -1$

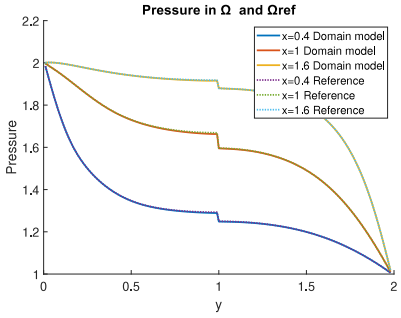

(f) Pressure in domain using using $\lambda = 2$ and

Fig. 3. Saturation for the whole domain and the reference model where the two-scaled model is used for different cases of κ and λ (left) and pressure for the domain at fixed x-values for different κ and λ (right). The saturations and pressures are compared to the reference solution in dotted lines.

dimensional model with the fracture flow model on the fracture surface coupled to the matrix flow equations. We adopt a domain decomposition procedure consisting of Neumann to Dirichlet and Dirichlet to Neumann operators for solving the model equations. Here we compute the fluxes from the matrix Ω_1 and Ω_2 at the interfaces, and compute the jump in the flux term and use this as a source term at the fracture domain. The equations for the fracture are solved with the boundary conditions at the fracture boundaries. The pressure calculated using the model equations in the fracture is used as the new Dirichlet boundary condition for Ω_1 and Ω_2. Then we repeat the procedure until the solution converges within tolerance.

In Fig. 2 we see that the effective model I gives a good prediction for the case where the permeability in the fracture is sufficiently large, $\lambda = -2, \kappa = -1$. The saturation curves from the upscaled model and the reference model are quite close to each other at each time step. We plot the pressure with respect to the y-axis for a fixed x coordinate. In the plot on the right side of Fig. 2, the three lines in the figure represent different fixed x-values in our domain Ω, and we plot the pressure with respect to the y-values. From Fig. 2(b) we see that the pressure curves from the upscaled model and the reference model overlap perfectly. However if we had tried this model for cases that are outside their range of validity λ and κ, for instance $\lambda > 0$, this model gives unphysical results. The upscaled models must be carefully selected depending on the values of λ and κ. We note that this effective model is derived under the assumption of high permeability in the fracture ($\lambda < 1$). This forces the pressure to be continuous across the fracture-matrix interface. However, for the two cases where $\lambda = 1$ and $\lambda = 2$, the permeability is small enough that it leads to discontinuity across the

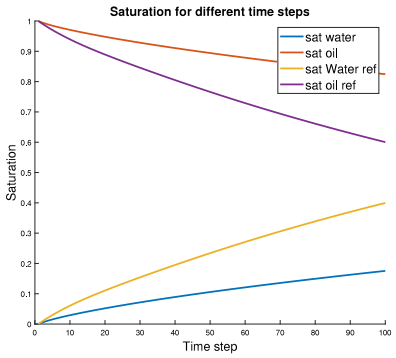

(a) Water and oil saturation in domain for the $\kappa = -1$. case where $\lambda = -2$ and $\kappa = -1$.

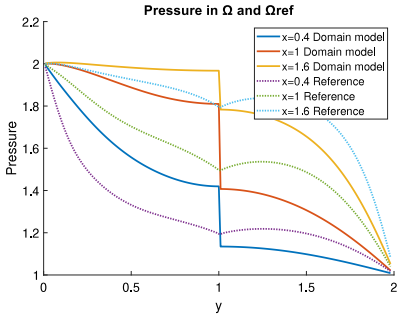

(b) Pressure in domain using using $\lambda = -2$ and

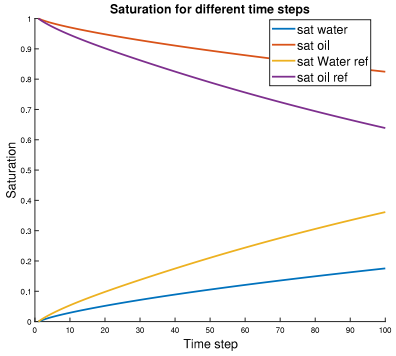

(c) Water and oil saturation in domain for the $\kappa = -1$. case where $\lambda = 1$ and $\kappa = -1$.

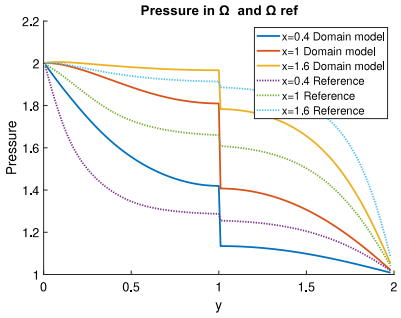

(d) Pressure in domain using using $\lambda = 1$ and

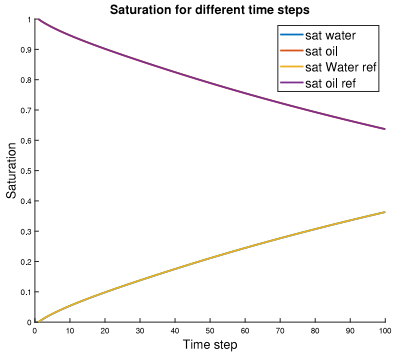

(e) Water and oil saturation in domain for the $\kappa = -1$. case where $\lambda = 2$ and $\kappa = -1$.

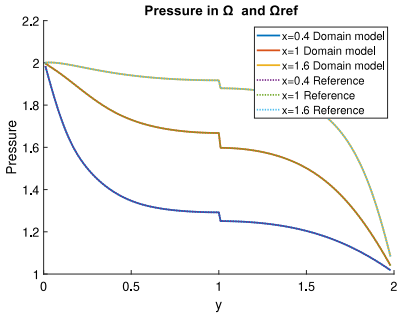

(f) Pressure in domain using using $\lambda = 2$ and

Fig. 4. Saturation for the whole domain and the reference model where the decoupled model is used for different cases of κ and λ (left) and pressure for the domain at fixed x-values for different κ and λ (right). The saturations and pressures are compared to the reference solution in dotted lines.

fracture-matrix interface. This explains why this model is unable to approximate the solutions in the other two cases.

5.2. Two-scaled model. Effective model V

For the two-scaled model, the solution procedure consists of rescaling the domain and then solve the fracture and the matrix domains in an implicit manner. Note that the interface conditions across the fracture-subdomain interface is continuity of pressures and that of fluxes. This implies that we can solve the fracture and subdomain unknowns together getting a system of algebraic equations where the subdomains and the rescaled fracture pressure unknowns are coupled together. In Fig. 3 we have used the upscaled model for various values of κ and λ. Again we use this model to solve the three cases as mentioned above.

In Fig. 3 we have plotted the saturation and pressure from our numerical results. We have used the two-scaled model and solved it for the three same λ and κ values as we have used in the previous model. From the previous section we expect the case where $\lambda = 1$ and $\kappa = -1$ to be the best fit for our model. This is also the case, as seen in Fig. 3(c), where the saturation curves overlap and we see the same for the pressure curves in Fig. 3(d). In the two other cases the fit is not as good. For the case where $\lambda = 2$ we see that the model does not catch the jump in pressure over the fracture. The two-scale model has the advantage that it resolves the flow profile inside the fracture unlike the other effective models that either take uniform pressure across the vertical direction or simply decouple the two subdomains. Since there

is a discontinuity of pressure across the fracture, this model seems to provide a better approximation for the case of $\lambda = 2$ (when there is also a discontinuity of pressures) than in the case when $\lambda = -2$ (when there is a continuity of pressures).

5.3. The decoupled model. Effective model VIII

Here we discuss the results from what we refer to as a decoupled model. The model is expected to work in cases where the fracture permeability is sufficiently small and refers to structures such as barriers, or cap rocks. In this upscaled model the two domains Ω_1 and Ω_2 are solved separately with zero-flux boundaries along the fracture interface. In this case, the effective problem decouples completely to give two inependent subproblems. Each of the subproblem is a two-phase model with zero-flux boundary at the fracture interface.. Fig. 4 gives the saturation and pressure curves for the upscaled model for the three cases as discussed above.

From Fig. 4 we see that this model gives a good matching for the saturation curves for cases where the permeability in the fracture is sufficiently low ($\lambda > 1$), Fig. 4(e). For the other cases in Fig. 4(a) and Fig. 4(c), we see that the saturation curves from the upscaled model and those from the reference solutions do not overlap. The pressures for our last time steps are shown in the graphs at the right hand side of Fig. 4, and we see the same type of behaviour here. The pressure curves from the upscaled model overlap with the pressures from the reference model for the case where $\lambda > 1$, Fig. 4(f). In the other cases however there is no overlapping, and the other upscaled model is therefore not good for predicting the flow in these intervals. Here, we note that the permeability is quite small obstructing the flow across the fracture interface and in the limit this leads to discontinuity of pressures across the matrix–fracture interface. This obstruction of flow is captured by the zero-flux condition. This explains why this effective model captures this case quite well but fails in the cases when the pressure is continuous (case i). Moreover, the critical case when $\lambda = 1$, even though it also leads to discontinuity of pressures, there is still flow taking place across the fracture surface and the pressures from the two subdomains sides are not independent rather coupled via a differential equation that resolves the pressure profile inside the fracture subdomain. This explains why this effective model is unable to approximate this case sufficiently well.

An important observation is that the model equations are discontinuous with respect to the parameters λ and κ. In particular, for $\lambda = 1$, we see that a small perturbation in this value would imply the upscaled model changes its character quite abruptly. This is not a satisfactory situation, because in practice we do not know the exact value of λ and κ. This suggests that higher order terms are needed to obtain the next order approximation so that the model equations retain the continuity. This would be the subject of our future investigations. This is also likely to give a better understanding of the practical use of mixed dimensional models for all the parameter ranges and using a fitting parameter to guess the pressure profile inside the fracture.

6. Conclusion

We consider a two-dimensional fractured porous medium where the fracture has a thickness ϵ. For our flow model we have considered a standard fully implicit two-phase oil/water model. This model consists of combining the mass balance equation with the Darcy equation for each of the two-phases. We perform an upscaling of the flow model which is obtained as the limit as ϵ tends to zero. The particularity in our approach is the scaling of the permeabilities of the two-phases and porosity of the matrix that is taken as exponents of ϵ characterized by two real numbers λ and κ respectively. We obtain a catalogue of models for different values of λ and κ. In our numerical simulations we show that we can use κ and λ to pick an upscaled model, and that the upscaled models work inside their range of validity. Finally, we think that the higher order approximations are needed in order to deal with the discontinuous nature of the upscaled models with respect to the parameters.

Declaration of competing interest

The authors declare that they have no known competing financial interests or personal relationships that could have appeared to influence the work reported in this paper.

Acknowledgements

We would like to thank the Norwegian research council for their financial support through the project RCN Project 811716 LAB2FIELD. All authors approved the version of the manuscript to be published.

References

Adler, P.M., Thovert, J.-F., 1999. Fractures and Fracture Networks, Vol. 15. Springer Science & Business Media.
Adler, P.M., Thovert, J.-F., Mourzenko, V.V., 2012. Fractured porous media. Oxford University Press.
Aghili, J., Brenner, K., Hennicker, J., Masson, R., Trenty, L., 2019. Two-phase discrete fracture matrix models with linear and nonlinear transmission conditions. GEM-Int. J. Geomath. 10 (1), 1.
Ahmed, E., Jaffré, J., Roberts, J.E., 2017. A reduced fracture model for two-phase flow with different rock types. Math. Comput. Simul. 137, 49–70.
Andersen, P., Evje, S., 2016. A model for reactive flow in fractured porous media. Chem. Eng. Sci. 145, 196–213.
Angot, P., Boyer, F., Hubert, F., 2009. Asymptotic and numerical modelling of flows in fractured porous media. ESAIM: Math. Model. Numer. Anal. 43 (2), 239–275.
Arbogast, T., Douglas, Jr., J., Hornung, U., 1990. Derivation of the double porosity model of single phase flow via homogenization theory. SIAM J. Math. Anal. 21 (4), 823–836.
Bastian, P., Chen, Z., Ewing, R.E., Helmig, R., Jakobs, H., Reichenberger, V., 2000. Numerical simulation of multiphase flow in fractured porous media. In: Chen, Z., Ewing, R.E., Shi, Z.-C. (Eds.), Numerical Treatment of Multiphase Flows in Porous Media: Proceedings of the International Workshop Held A Beijing, China, 2–6 August 1999. Springer Berlin Heidelberg, Berlin, Heidelberg, pp. 50–68.
Bear, J., 1988. Dynamics of fluids in porous media. Dover Publications, INC.
Berre, I., Doster, F., Keilegavlen, E., 2019. Flow in fractured porous media: A review of conceptual models and discretization approaches. Transp. Porous Media 130 (1), 215–236.
Boon, W.M., Nordbotten, J.M., Vatne, J.E., 2017. Functional analysis and exterior calculus on mixed-dimensional geometries. arXiv preprint arXiv:1710.00556.
Brenner, K., Groza, M., Guichard, C., Masson, R., 2015. Vertex approximate gradient scheme for hybrid dimensional two-phase Darcy flows in fractured porous media. ESAIM: Math. Model. Numer. Anal. 49 (2), 303–330.
Brenner, K., Hennicker, J., Masson, R., Samier, P., 2018. Hybrid-dimensional modelling of two-phase flow through fractured porous media with enhanced matrix fracture transmission conditions. J. Comput. Phys. 357, 100–124.
Bukač, M., Yotov, I., Zunino, P., 2015. An operator splitting approach for the interaction between a fluid and a multilayered poroelastic structure. Numer. Methods Partial Differential Equations 31 (4), 1054–1100.
Bukac, M., Yotov, I., Zunino, P., 2016. Dimensional model reduction for flow through fractures in poroelastic media. ESAIM: Math. Model. Numer. Anal..
Carmeliet, J., Delerue, J.-F., Vandersteen, K., Roels, S., 2004. Three-dimensional liquid transport in concrete cracks. Int. J. Numer. Anal. Methods Geomech. 28 (7–8), 671–687.
Dugstad, M., Kumar, K., Pettersen, Ø., 2021. Dimensional reduction of a fractured medium for a polymer EOR model. Comput. Geosci. 1–21.
Formaggia, L., Fumagalli, A., Scotti, A., Ruffo, P., 2014. A reduced model for Darcy's problem in networks of fractures. ESAIM: Math. Model. Numer. Anal. 48 (4), 1089–1116.
Fountain, A.G., Walder, J.S., 1998. Water flow through temperate glaciers. Rev. Geophys. 36 (3), 299–328.
Fumagalli, A., Keilegavlen, E., Scialò, S., 2019. Conforming, non-conforming and non-matching discretization couplings in discrete fracture network simulations. J. Comput. Phys. 376, 694–712.
Fumagalli, A., Scotti, A., 2013. A numerical method for two-phase flow in fractured porous media with non-matching grids. Adv. Water Resour. 62, 454–464.
Gahn, M., Neuss-Radu, M., Knabner, P., 2016. Homogenization of reaction–diffusion processes in a two-component porous medium with nonlinear flux conditions at the interface. SIAM J. Appl. Math. 76 (5), 1819–1843.
Gahn, M., Neuss-Radu, M., Knabner, P., 2018. Effective interface conditions for processes through thin heterogeneous layers with nonlinear transmission at the microscopic bulk-layer interface. Netw. Heterog. Media 13 (4), 609.

Gander, M.J., Hennicker, J., Masson, R., 2021. Modeling and analysis of the coupling in discrete fracture matrix models. SIAM J. Numer. Anal. 59 (1), 195–218.
Gerritsen, M.G., Durlofsky, L.J., 2005. Modeling fluid flow in oil reservoirs. Annu. Rev. Fluid Mech. 37, 211–238.
Girault, V., Kumar, K., Wheeler, M.F., 2016. Convergence of iterative coupling of geomechanics with flow in a fractured poroelastic medium. Comput. Geosci. 20 (5), 997–1011.
Helmig, R., et al., 1997. Multiphase Flow and Transport Processes in the Subsurface: a Contribution to the Modeling of Hydrosystems. Springer-Verlag.
Hoteit, H., Firoozabadi, A., 2008. An efficient numerical model for incompressible two-phase flow in fractured media. Adv. Water Resour. 31 (6), 891–905.
Kim, J.-G., Deo, M.D., 2000. Finite element, discrete-fracture model for multiphase flow in porous media. AIChE J. 46 (6), 1120–1130.
Kumar, K., List, F., Pop, I.S., Radu, F.A., 2020. Formal upscaling and numerical validation of unsaturated flow models in fractured porous media. J. Comput. Phys. 407, 109138.
Lie, K.-A., 2019. An Introduction to Reservoir Simulation Using MATLAB/GNU Octave: user Guide for the MATLAB Reservoir Simulation Toolbox (MRST). Cambridge University Press.
List, F., Kumar, K., Pop, I.S., Radu, F.A., 2020. Rigorous upscaling of unsaturated flow in fractured porous media. SIAM J. Math. Anal. 52 (1), 239–276.
Martin, V., Jaffré, J., Roberts, J.E., 2005. Modeling fractures and barriers as interfaces for flow in porous media. SIAM J. Sci. Comput. 26 (5), 1667–1691.
Morales, F., Showalter, R.E., 2010. The narrow fracture approximation by channeled flow. J. Math. Anal. Appl. 365 (1), 320–331.
Morales, F., Showalter, R.E., 2012. Interface approximation of Darcy flow in a narrow channel. Math. Methods Appl. Sci. 35 (2), 182–195.
National Research Council, et al., 2001. Conceptual Models of Flow and Transport in the Fractured Vadose Zone. National Academies Press.
Neuss-Radu, M., Jäger, W., 2007. Effective transmission conditions for reaction-diffusion processes in domains separated by an interface. SIAM J. Math. Anal. 39 (3), 687–720.
Pop, I.S., Bogers, J., Kumar, K., 2017. Analysis and upscaling of a reactive transport model in fractured porous media with nonlinear transmission condition. Vietnam J. Math. 45 (1–2), 77–102.
Pruess, K., Narasimhan, T., 1982. A practical method for modeling fluid and heat flow in fractured porous media.
Reichenberger, V., Jakobs, H., Bastian, P., Helmig, R., 2006. A mixed-dimensional finite volume method for two-phase flow in fractured porous media. Adv. Water Resour. 29 (7), 1020–1036.
Singh, G., Pencheva, G., Kumar, K., Wick, T., Ganis, B., Wheeler, M.F., et al., 2014. Impact of accurate fractured reservoir flow modeling on recovery predictions. In: SPE Hydraulic Fracturing Technology Conference. Society of Petroleum Engineers.
Smith, I., Landis, E., Gong, M., 2003. Fracture and Fatigue in Wood. John Wiley & Sons.
Tunc, X., 2012. La Modélisation Des Failles Conductrices Pour Les Écoulements En Milieux Poreux (Ph.D. thesis). Université De Provence.
van Duijn, C., De Neef, M., 1998. Similarity solution for capillary redistribution of two phases in a porous medium with a single discontinuity. Adv. Water Resour. 21 (6), 451–461.
van Duijn, C.J., Eichel, H., Helmig, R., Pop, I.S., 2007. Effective equations for two-phase flow in porous media: the effect of trapping on the microscale. Transp. Porous Media 69 (3), 411–428.
Watanabe, U., Imamura, Y., Iida, I., 1998. Liquid penetration of precompressed wood VI: anatomical characterization of pit fractures. J. Wood Sci. 44 (2), 158–162.